CZECH TECHNICAL UNIVERSITY IN PRAGUE

FACULTY OF BIOMEDICAL ENGINEERING
Department of Biomedical Technology

Brain Tumors Heating by Microwave Hyperthermia

Ohřev mozkových nádorů pomocí mikrovlnné hypertermie

Master thesis

Study programme:	Biomedical and Clinical Engineering
Study branch:	Biomedical Engineering
Supervisor of the master thesis:	doc. Ing. David Vrba, PhD.

Bc. Gabriela Liptáková

Kladno 2022

MASTER'S THESIS ASSIGNMENT

I. PERSONAL AND STUDY DETAILS

Student's name:	**Liptáková Gabriela**	Personal ID number:	**465434**
Faculty:	**Faculty of Biomedical Engineering**		
Department:	**dept**		
Study program:	**Biomedicínské inženýrství**		

II. MASTER'S THESIS DETAILS

Master's thesis title in English:

Brain Tumors Heating by Microwave Hyperthermia

Master's thesis title in Czech:

Ohřev mozkových nádorů pomocí mikrovlnné hypertermie

Guidelines:

In COMSOL Multiphysics platform perform a 2D analysis of the antenna count and their working frequency on the ability to expose tumor tissue with an electromagnetic field. Evaluate this analysis according to the Directive ESHO. Design an antenna element meeting the dimensional requirements of the 2D analysis. Measure the radiation characteristics of this antenna element and compare them with simulations.

Bibliography / sources:

[1] J. Vrba, Lékařské aplikace mikrovlnné techniky, ed. 1st, ČVUT Praha, 2003, ISBN 80-01-02705-8
[2] C. A. Balanis, Advanced Engineering Electromagnetics, ed. Solution Manual, Wiley, 1989, Chapter 2, ISBN 0471621943
[3] Trefna, HD at al., Quality assurance guidelines for superficial hyperthermia clinical trials, STRAHLENTHERAPIE UND ONKOLOGIE, ročník 193, číslo 5, 2017, Květen, 351-366 s.

Name of master's thesis supervisor:

doc. Ing. David Vrba, Ph.D.

Name of master's thesis consultant:

prof. Dr.-Ing. Jan Vrba, M.Sc.

Date of master's thesis assignment: **14.02.2022**
Assignment valid until: **22.09.2023**

doc. Ing. Martin Rožánek, Ph.D.	prof. MUDr. Jozef Rosina, Ph.D., MBA
Head of department	Dean

DECLARATION

I hereby declare that I have completed this thesis with the topic "Brain Tumors Heating by Microwave Hyperthermia" independently and that I have attached an exhaustive list of citations of the employed sources.

I do not have a compelling reason against the use of the thesis within the meaning of Section 60 of the Act No. 121/2000 Sb., on copyright, rights related to copyright and amending some laws (Copyright Act).

In Kladno Bc. Gabriela Liptáková

ACKNOWLEDGEMENTS

I wish to express my sincere gratitude to my supervisor, doc. Ing. David Vrba, PhD. for providing me guidance and valuable advice throughout the whole research and mainly during the design and experiment phase of the thesis. I would also like to thank prof. Dr.-Ing. Jan Vrba, M.Sc., Ing. Jan Rédr, and Ing. Tomáš Pokorný for their dedicated time and effort in helping me with the simulation settings.

ABSTRACT

Brain Tumors Heating by Microwave Hyperthermia

The aim of this Master's thesis is a numerical study of the feasibility of microwave hyperthermia of brain tumours. The study analysed the ability to achieve therapeutically relevant constructive superposition of electromagnetic waves in treatment targets depending on the size and position of the targets, the operating frequency of the hyperthermic system, and the number of antenna elements forming the applicator. This study was performed for a total of 10 anatomically realistic human head models, in which 10 tumour models with diameters of 2, 2.5, and 3 cm were considered. Applicators with 8, 12, 16, and 24 antenna elements and operating frequencies of 434, 650, 915, and 1150 MHz were analysed. For all scenarios, the distribution of electromagnetic fields from individual antenna elements was calculated and treatment planning was performed, and its quality was evaluated using parameters used in current clinical practice TC and HTQ. Both parameters indicate optimal treatment for an operating frequency of 434 MHz. A sufficient number of antenna elements meeting the requirements to cover the entire target area is 12 and increasing their number does not have a significant effect on the quality parameters. For the resulting operating frequency of 434 MHz, an antenna element was further designed, implemented, and tested, which proved to be able to deliver sufficient power to the tissue in accordance with the simulations.

Keywords:

Hyperthermia, brain tumours, dipole antennas

ABSTRAKT

Ohřev mozkových nádorů pomocí mikrovlnné hypertermie

Cílem této diplomové práce je numerická studie proveditelnosti mikrovlnné hypertermie nádorů mozku. V rámci studie byla provedena analýza schopnosti dosáhnout terapeuticky relevantní konstruktivní superpozice elektromagnetických vln v cílech léčby v závislosti na velikosti a pozici cílů, pracovní frekvenci hypertermického systému, počtu anténních elementů tvořící aplikátor. Tato studie byla provedena pro celkem 10 anatomicky realistických modelů lidské hlavy, ve kterých bylo uvažováno 10 modelů nádorů o průměrech 2, 2,5 a 3 cm. Byly analyzovány aplikátory s 8, 12, 16 a 24 anténními elementy a pracovní frekvence 434, 650, 915 a 1150 MHz. Pro všechny scénáře byly vypočítány rozložení elektromagnetických polí od jednotlivých anténních elementů a bylo provedeno plánování léčby a vyhodnocena jeho kvalita pomocí parametrů využívaných v aktuální klinické praxi TC a HTQ. Oba parametry indikují optimální léčbu pro pracovní frekvenci 434 MHz. Dostatečný počet anténních elementů, splňující požadavky na pokrytí celé cílené plochy, je 12 a zvýšením jejich počtu nemá na kvalitativní parametry výrazný vliv. Pro výslednou pracovní frekvenci 434 MHz byl dále navržen, realizován a testován anténní element, který prokázal schopen dodávat dostatečný výkon do tkáně v souladu se simulacemi.

Klíčová slova

Hypertermie, mozkové nádory, dipólové anteny

Table of Contents

List of Symbols and Abbreviations

List of Symbols

Symbol	Unit	Meaning
S_{11}	dB	Scattering parameter
ρ	kg/m^3	Density
μ_r	-	Relative permeability
E	V/m	Electric field intensity
k_0	-	Wave number of free spaces
ε_r	-	Relative permeability
σ	S/m	Electrical conductivity
ε_0	F/m	Permittivity of the vacuum
SAR	W/kg	Specific Absorption Rate
TC25	%	Tumour Coverage by 25% of the highest iso-SAR values
TC50	%	Tumour Coverage by 50% of the highest iso-SAR values
TC75	%	Tumour Coverage by 75% of the highest iso-SAR values
HTQ	-	Hotspot-to-Target Quotient
f	Hz	Frequency

List of Abbreviations

Abbreviation	Meaning
HT	Hyperthermia
EM	Electromagnetic
GM	Glioblastoma Multiforme
RT	Radiotherapy
RF	Radiofrequency
MW	Microwave
ESHO	European Society of Hyperthermic Oncolohy
SAR	Specific Absorption Rate
IR	Infrared
US	Ultrasound
MRI	Magnetic Resonance Imaging
CSF	Cerobrospinal Fluid
UV	Ultraviolet
PEC	Perfect Electric Conductor
TC	Target Coverage
HTQ	Hotspot-to-Target Quotient
IEEE	Institute of Electrical and Electronics Engineers

1 Introduction

Hyperthermia (HT), defined as an induced temperature rise of 40–44 °C, has been proven to improve the therapeutic success of conventional treatment modalities for brain tumours, such as radiotherapy and chemotherapy [1; 2; 3]. Microwave (MW) HT uses applicators to provide electromagnetic (EM) energy to the body. These applicators use antennas that primarily operate in the lower half of the ultra-high frequency band to achieve adequate penetration. Antennas are often deployed in an annular phased array configuration of multiple antenna elements around the patient's head. The positive wave interference process is used to achieve localized power deposition in the tumour. In other words, the focal point can be directed to target the tumour by using varied amplitudes and phases at the antennas' feeding locations. The design of the antenna element is the essential part of the HT device and should fulfil standard requirements which are described in the quality guidelines developed by the European Society for Hyperthermic Oncology [4]. Generally, the requirements are small dimensions, a reflection coefficient better than -10 dB and the capability of handling the power of at least 150 W.

The aim of current studies is to find the ideal operating frequency of the HT system, which would achieve sufficient power deposition of the target area while minimising the delivery of power in the hotspots of healthy tissues. Lower frequencies penetrate deeper into the tissue, but their wider wavelength causes unwanted heat deposits in surrounding healthy tissues [5].

Another approach considered in the development of HT systems is the ideal number of antenna elements around the head. While increasing the number of antenna elements, EM energy coupled to the wanted target is elevated as well, the objective is to find an ideal balance of the element number for manufacturing a financially appropriate system. [6]

2 Overview of the Current State

2.1 Brain Tumours

A brain tumour is an abnormal growth of cells that occurs in the brain. Like other tumours, brain tumours can be benign or malignant. The latter grow much more rapidly than benign tumours and frequently spreads into surrounding brain tissue. The former tends to grow slowly and does not typically disperse. Only malignant tumours are considered cancerous, but a benign brain tumour can still be problematic as its growth can impact surrounding brain tissue. If a brain tumour begins in the brain, it's called a primary brain tumour. If it spreads to the brain from some other location, it is known as a secondary brain tumour. [7]

The symptoms of brain tumours vary depending on what part of the brain is impacted and thus from case to case, but some common symptoms include headache, nausea and vomiting, sensory disturbances like blurred vision, loss of consciousness, confusion, and cognitive changes [8]. We differentiate between adult and child tumours. Children tend to get different tumours such as pilocytic astrocytoma, malignant gliomas, medulloblastomas, or ependymomas while typical adult brain tumours include glioblastoma multiforme, oligodendroglioma, and meningioma [9].

Gliomas are a category of brain tumours that begin in glial cells. The most common glioma is an astrocytoma, which arises from the glial cells called astrocytes. One example of an astrocytoma is a low-grade astrocytoma, which indicates a slow-growing tumour that is usually benign [9]. Another example, however, is glioblastoma multiforme (GM), which is a highly malignant tumour that grows rapidly and spreads aggressively. In radiology imaging, we can see that GM crosses the midline of the corpus callosum and creates a butterfly shape, sort of symmetrical on the midline. Cells of GM are categorised as pseudo palisading tumour cells and are associated with necrosis [10]. Meningiomas are the most common primary brain tumour of arachnoid shape. They form in the meninges and are usually benign and superficially located. From a histology point of view, their cells are prone to calcification which creates a pattern similar to rings on a tree. Oligodendrogliomas are quite rare and appear mostly in the frontal lobe and their cells have a typical fried egg appearance with round nuclei and clear cytoplasm. They tend to calcify as well as meningiomas [11].

A study [12] concluded in Finland on 331 adults provided the incidence of the most recurring tumours according to their most frequent positions in the brain. Apart from the location analysis, the study concluded that the patients suffering from the glioma brain tumours develop with the highest probability (47 %) a multiform glioblastoma. The second most frequent glioma tumour is astrocytoma with the occurrence of 23 %.

Tumours are often diagnosed in the following brain lobes:

1. Frontal lobe with the incidence of 40 %
2. Temporal lobe with the incidence of 29 %
3. Parietal and Occipital lobe with the incidence of 17 %

The mean volume of head tumours measured from the magnetic resonance (MR) scans was 19.67 ± 13.73 cm^3 [13]. The great variance of the values indicates that the size of the tumours is vastly influenced by the time at which it was diagnosed and the aggressiveness of the tumour type.

2.2 Hyperthermia

Hyperthermia is a compelling sensitiser of ionising radiation which is now a standard way of cancer treatment. Radiative treatment is always aggressive and lowers the quality of life for the patients suffering from cancer. It is combined with chemotherapy, specifically for brain tumours, and temozolomide is used. [14]

A trial based on comparing of survival probability of 112 patients showed that the combination of hyperthermia and radiotherapy tends to double the tumour response rate (increasing 2-year survival from 15 % to 31 %). This trial was performed for patients with recurrent head tumours, including GM, squamous cell carcinoma or melanoma. The radiotherapy used was brachytherapy, delivering radiation directly to the target volume. [15]

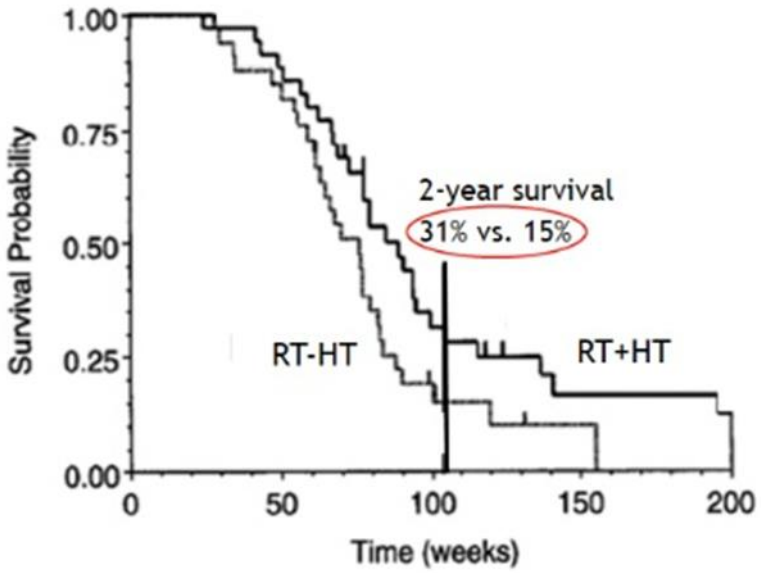

Figure 2.1: Comparison of 2-year survival rate of patients treated with radiotherapy and patients treated with the combination of radiotherapy and hyperthermia [15]

During HT, tissue is heated to a temperature of 40 to 44 ° for 60 to 90 minutes. This temperature range causes protein denaturation in cells and subsequent aggregation of nuclear, cytoplasmic or membrane proteins. While there is certain thermotolerance enhanced by Heat shock proteins in mammalian cells, the tumour cells are way more sensitive to changes in temperature and therefore its low tolerance makes them vulnerable to hyperthermia. For the progression of the tumour, it is essential to sustain a rich blood supply which acts as a source of oxygen and nutrients. This vasculature around the tumour is more sensitive than healthy tissue. The vascular stasis in human tissue begins at 47 °C while in tumour cells it is induced at 41–42 °C. Consequently, blood circulation is topped and therefore the tumour loses its vital dosage of nutrients, necessary for its manifestation. Moreover, it enhances the effectiveness of radiation in synergic interaction called heat or thermal sensitisation. [16] When hyperthermia is applied before the radiation, tumour cells can be sensitised for up to several hours. The aim of current research in the field of cancer treatment is to minimise long-term side effects and rise the survival prognosis for the patients. There are no late toxicity effects of HT found. [3]

Adding HT to standard therapy shows an overall response of 54.9 % compared with the response of 39.8 % for the sole radiotherapy. This prognosis is based on the outcome of 38 clinical trials in [3]. Based on the summary of complete local tumour control reported by randomised clinical studies for various tumour locations, comparing radiotherapy and radiotherapy with regional HT, I present the following graph, which shows the positive outcome of adding hyperthermia to the standard process of cancer treatment.

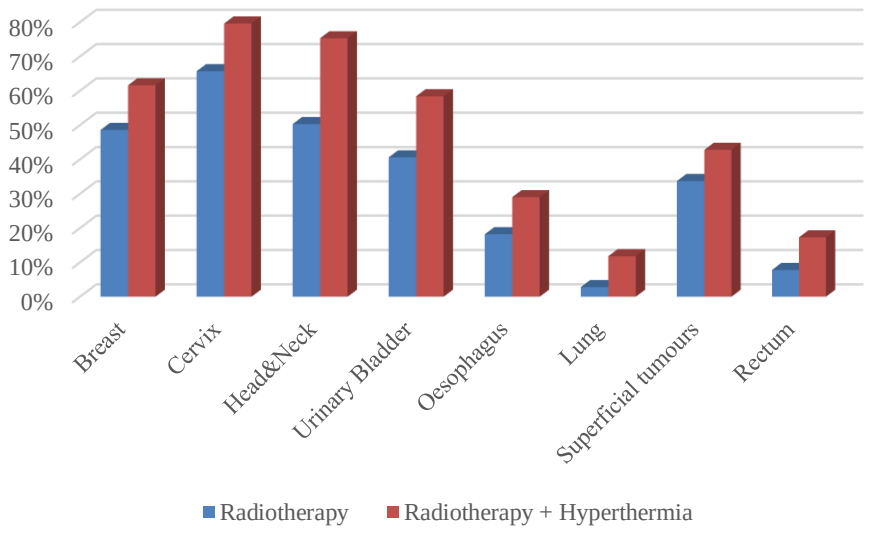

Figure 2.2: Complete response of the treatment with radiotherapy and combination of hyperthermia and radiotherapy for chosen cancer occurrence

Based on the data from 9 clinical trials of head and neck cancer, the complete response of RT and RT+HT treatment was 50.3 % and 75.3 % respectively.

2.3 Microwave heating

Electromagnetic-based methods, such as radiofrequency (RF) and microwave (MW) are now studied for their controlled heating effects on biological tissues. This thesis summarises the positives of microwave hyperthermia, its effectiveness, and its limitations on the treatment of brain tumours. It shows the correlation of frequency and number of antennas used on localised heating quality. To evaluate this quality, the results of simulations were graded according to the standards recommended by the European Society of Hyperthermic Oncology (ESHO). The main difference between electromagnetic-based technologies is the used frequency of the applicator. We can divide them into three major groups: radiofrequency, operating at the frequency range from 300 Hz to 300 MHz, microwave with a range from 300 MHz to 300 GHz and infrared technology spanning from 300 GHz to 4300 THz [17]. This covers the microwave technologies and their heating capabilities. At the frequency range of microwaves, all tissues in the human body behave as lossy dielectrics, which means they act as poor conductors and insulators. Increasing the frequency of electromagnetic waves above 100 MHz causes oscillation of polar water molecules which causes mechanical friction. These molecules oscillate 100 million cycles per second in the electric field and thus, the heating is generated. This is characterised as a radiative mode of propagation [18].

For the effect of EM fields in biological tissues, we use describing parameters as effective electrical conductivity σ (unit S/m) and relative permittivity ε_r (unitless). While the former represents all electrical losses in the tissue due to the varying currents driven by the EM field, relative permittivity specifies the ability to polarise a tissue exposed to the EM field. Both characteristics are varying with the tissue type (characterised by density, amount of water, etc.), temperature and frequency. A comprehensive database, including thermal parameters of human tissues, is accessible in the IT'IS Tissue Properties Database. [19]

The energy which is absorbed in tissue can be expressed using the parameter of Specific Absorption Rate (SAR) with units of W/kg, representing the EM energy absorbed by the tissue. It is directly proportional to the specific heat capacity and there is a direct correlation between the SAR parameter and the temperature rise in the tissue with the thermal conduction and thermal convection being neglected. The heat which is transported in the tissue is typically calculated with the Pennes Bioheat model. The limitation of this equation is that it neglects the direction of blood flow or vasculature which often change the temperature distribution in the heating region. This is why there are currently new models being developed, such as the discrete vasculature model. [20]

2.4 ESHO directive

The aim of each treatment plan is the choice of the right hyperthermia technique as no one size fits for all. For this purpose, the part of this thesis is the evaluation of

techniques according to the standards of the European Society for Hyperthermic Oncology (ESHO). Its main objective is to promote for the standard quality-assuring parameters of each heating modality whether it is superficial or interstitial hyperthermia. The latter, the intraluminal HT technique deals with invasive techniques, as they are manufactured to deliver hyperthermic temperatures within a tumour mass. These include brachytherapy or catheter implantation. In my thesis, I deal with deep-seated tumours located in the brain, exposed by external devices which are minimally or non-invasive for the patient. Like other heating technologies, the aim of deep hyperthermia is to couple the energy in the target area to heat it to temperatures of 42 to 45 °C while preserving surrounding healthy tissues. Using only one antenna element with a single adjustable power controller would not be sufficient to deliver energy into deeper layers, that is why phased-array applicators are used. Each element of the array has its own power control which enables the power steering.

2.4.1 Evaluation quality indicators of treatment

There are several parameters used for describing the outcome of hyperthermia treatment planning. Each one of the parameters is based on SAR evaluation. As the heat is a function of temperature and time, it is also important to comprise the duration of HT in the treatment planning.

Thermal dose parameters

CEM43°C is the cumulative number of equivalent minutes at a temperature of 43 °C. [21]

Target coverage (TC)

The desired coverage and THQ are regarded as quality indicators. The target coverage has been assessed at the 25%, 50%, 75% (TC25/TC50/TC75) level, and is defined as the volume percentage of the hyperthermia treated volume covered by a 25%, 50%, 75% iso-SAR value when the SAR distribution is normalized to the maximum SAR in the complete patient model. For example, a TC25 of 50% means that the normalized SAR distribution in one half of the hyperthermia treated area is 0,25. [22]

THQ

Hotspot quotient ratio is defined as the ratio of the average SAR in the first percentile of highest SAR values in healthy tissues to the average SAR in the tumour. HTQ is used as the goal function for PS optimisation of SAR distribution in HT treatment planning. [22]

2.4.2 Electromagnetic radiative heating

In radiative electromagnetic HT, the interference of waves enables the heating of deeply localised tumours and focuses the heat delivery to a predefined volume. These applicators operate at frequencies higher than 400 MHz, while the exact value depends on the penetration depth. This is due to the electric properties of individual tissues, such as electric conductivity or permittivity. Radiating heating strategy is used both for superficial and deep-seated tumours. The depths we can reach are one to two centimetres by infrared heating, 2 cm with 2450 MHz, and approximately 3 cm with 915 MHz, which is standardly used in the USA. The frequency of 434 MHz is most widely used in Europe, it can penetrate through 4 cm of tissue. For deep-seated cancer, radiofrequency waves are used, typically from 70 to 140 MHz. For this range, it is always required to use multiple antennas as the range does not supply the centimetre-scale spatial control [23]. But what the antenna should fulfil? It ought to be capable of delivering a symmetrical radiation pattern with a reflection coefficient better than -10 dB in the whole frequency band. The best antennas are electromagnetically compatible, as it is still believed and proven that magnetic resonance imaging and thermometry technique is the most appropriate.

Other hyperthermia systems are electromagnetic capacitive heating systems, ultrasound, and infrared radiation. [4]

Scattering parameters

The object of developing an ideal antenna is to correctly design its parameters. The ability of a radiating element to deliver adequate energy into the tissue is determined by its frequency, size, and the medium in which it is placed. The aim is to minimise the reflection of power back into the generator, which means we must adapt the impedance of the electromagnetic wave. The ratio describing the value which is reflected into the generator and is therefore not applied to the tissue is a *Scattering Parameter* or S-parameter. Generally, it expresses how the EM wave is propagated through a medium, therefore it characterises a part of the circuit without the knowledge of its inner arrangement. S-parameter is a complex number often expressed in subscripts S_{ij} where i stands for the output port and j is for the port that is excited or the input port. Thus, parameter S_{11} which will be expressed in this thesis stands for the ratio of the signal's amplitude that reflects from the first port to the signal's amplitude incident on this port. If we take a two-port system, its S-parameters are written in a matrix structure, with reflection coefficients along the diagonal and transmission coefficients are placed off-diagonal.

In the following picture, a two-port network is presented. Variables a_i represent a wave incident to port i and variables b_j represent reflected waves from port j. The magnitudes of the mentioned variables may be referred to as voltage-like variables, normalised by a specified reference impedance Z_0. In the case of measuring systems, the impedance is set to 50 Ω.

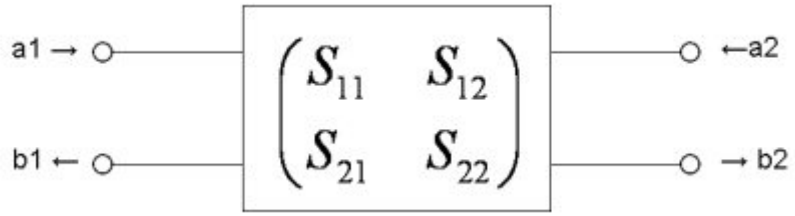

Figure 2.3: A two-port network with marked waves of incidence and reflection

3 Aims of Thesis

The aim of this thesis is to evaluate the frequency and number of antennas used for microwave hyperthermia of head tumours. Based on the best scenario of power deposition, the ideal frequency and the antenna count is obtained using optimisation of chosen parameters (amplitude, phase, SAR). From the results, the ideal antenna element is to be designed with chosen frequency and parameters.

For the analysis there are the following steps to be taken:

1. Development of 2D head models from ten real patient models using segmentation of magnetic resonance images
2. Electromagnetic field simulations of chosen antennas
3. Optimisation of power deposition parameters for chosen frequencies, localisations of tumours and number of antennas used
    a.
4. Design of antenna array with an estimated frequency
5. Practical experiment in the laboratory of FBMI CTU establishing the reflection of EM radiation of the designed antenna

4 Methods

In this chapter, I summarise the approaches of frequency and number of antenna analyses for the best treatment outcome. For a more coherent narration, I present the following graph describing the steps taken and the software used for each of them.

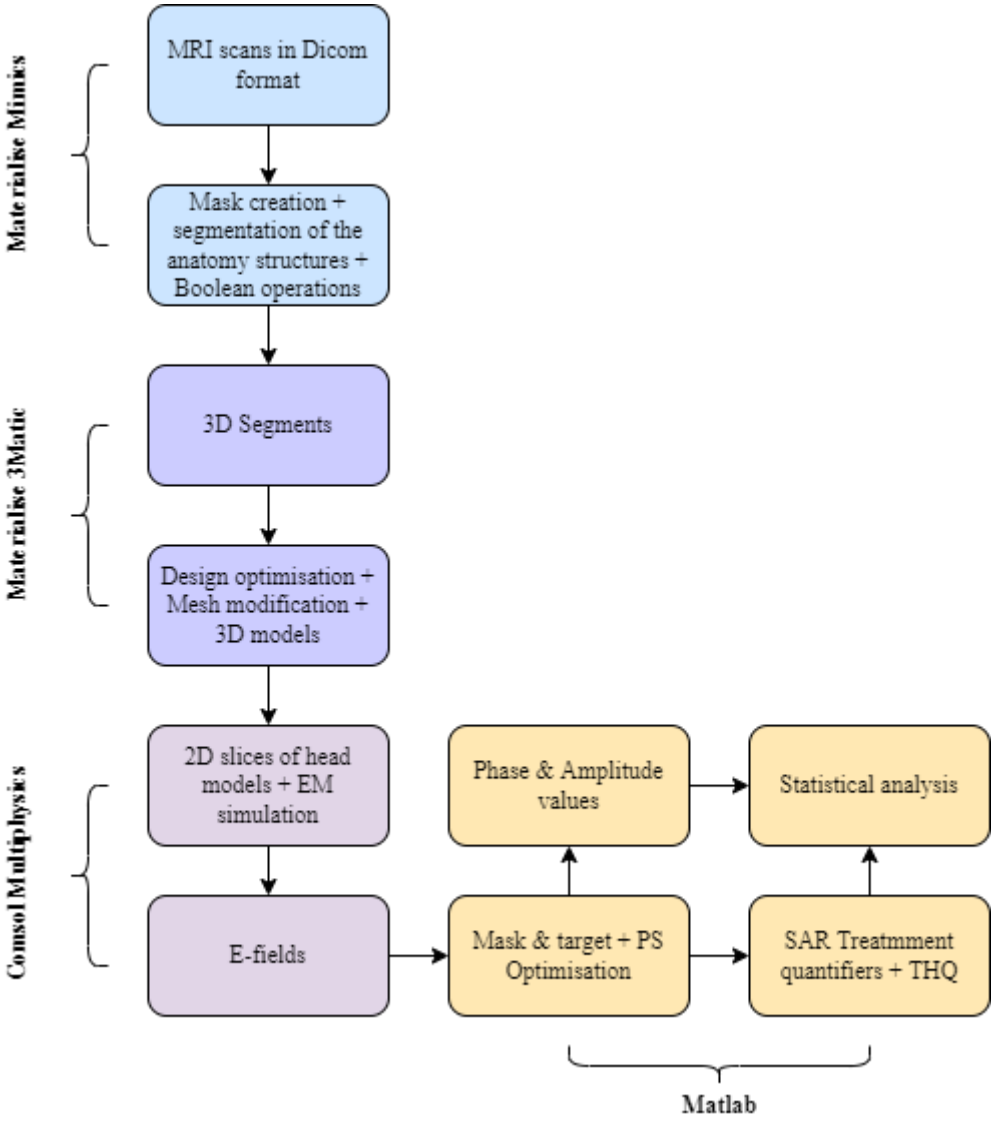

After the analysis, it was necessary to design antenna with chosen parameters, based on the calculations provided by Optimisation and the research summarised in the previous chapters. In COMSOL Multiphysics, a bow-tie antenna was designed and later manufactured. For the measurement we use the equipment of the school laboratory, including cSAR3D developed by SPEAG.

4.1 Collection of patients' head models

To create 2D models representing slices of human head, at first it was necessary to acquire segmented images of human brain. This was obtained using MRI images of real patients which were later processed using Materialise Mimics for segmentation and Materialise 3Matic for the reconstruction of head models. After this reconstruction, simplified models with basic tissues were converted to the file format compatible with COMSOL software. Using a *Plane extractor* in COMSOL we obtained the contours of selected tissues in the human brain which were later used for the simulations in MATLAB.

4.1.1 Segmentation

Before segmentation, I pre-processed MRI acquired images using contrast and brightness tools. After completion of image adjustment, it was necessary to threshold a mask, which would include the selected tissue. Using the 3D viewer tool, I treated each selected tissue to remove redundant voxels or connect incomplete areas. For the outer shells of the scalp (skin + fat + muscles), I chose the morphological operation of dilatation so that after subtracting other inner tissues from this layer I would not lose its thickness. Afterwards, with the finalisation of the scalp layer, I continued with the skull, cerebrospinal fluid, and inner mass of the brain, which includes white matter and grey matter. It was obtuse to split these two inner layers from each other as there is only a thin and non-homogenous stratum of grey matter, that is why I chose single geometry for them. For simulations, mean values of density and electric conductivity will be used for grey and white matter. MIMICS offers tools of Boolean algebra operations which were used for adding and subtracting one layer from another. I used these operations only to estimate the thickness of tissues so that after the subtraction there would not be non-consistent overlays.

4.1.2 3D models

After completing, individual segments were loaded into Materialise 3-Matic, software analysis, and design, where segmented models were further edited to eliminate surface imperfections. *Wrapping* was used to fill holes and create a smooth surface and for a further level of the smooth watertight surface, *Smoothing* tool was used. The domains of interest were divided into small segments using mesh. We can characterise mesh as a discretisation of domains existing in one, two, or three dimensions. In our case, 3D meshes created for numerical analysis consist of tetrahedra, hexahedra, pyramids, and prisms. Final mesh can be generated for finite element analysis which is used in COMSOL Multiphysics. Other required steps for simulations include boundary conditions and material selection.

4.2 Electric field simulations

For the study of electric fields, our 3D models of the head were imported in COMSOL Multiphysics and using a *Plane extractor* in the widest and longest part of the head, ten 2D slices were created.

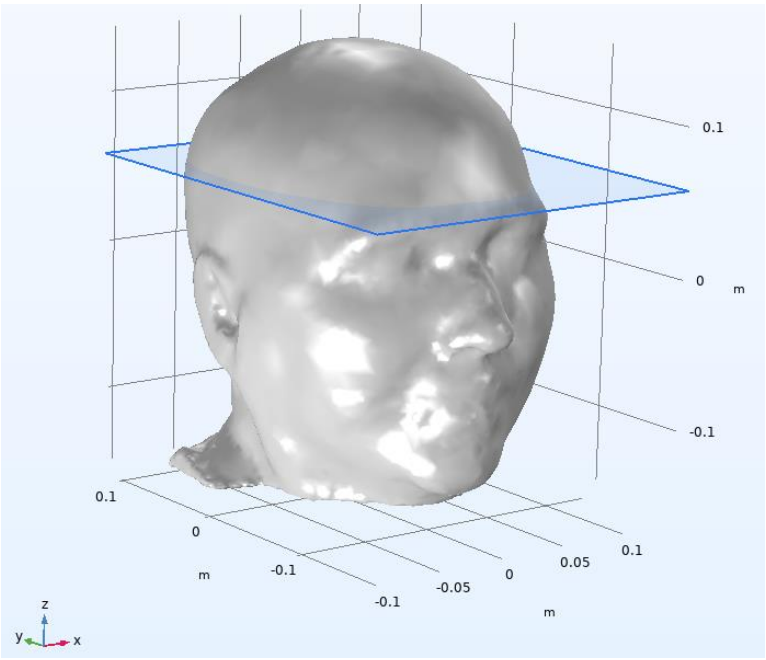

Figure 4.1: Model of the patient with marked plane for the extraction of 2D slice

These ten patients' models alter in the size and ratio of each domain. Subsequently, antennas were deployed around the scalp in an elliptical domain, representing an adaptive medium. There were four scenarios of antenna layout, 24, 16, 12 and 8 dipole formations.

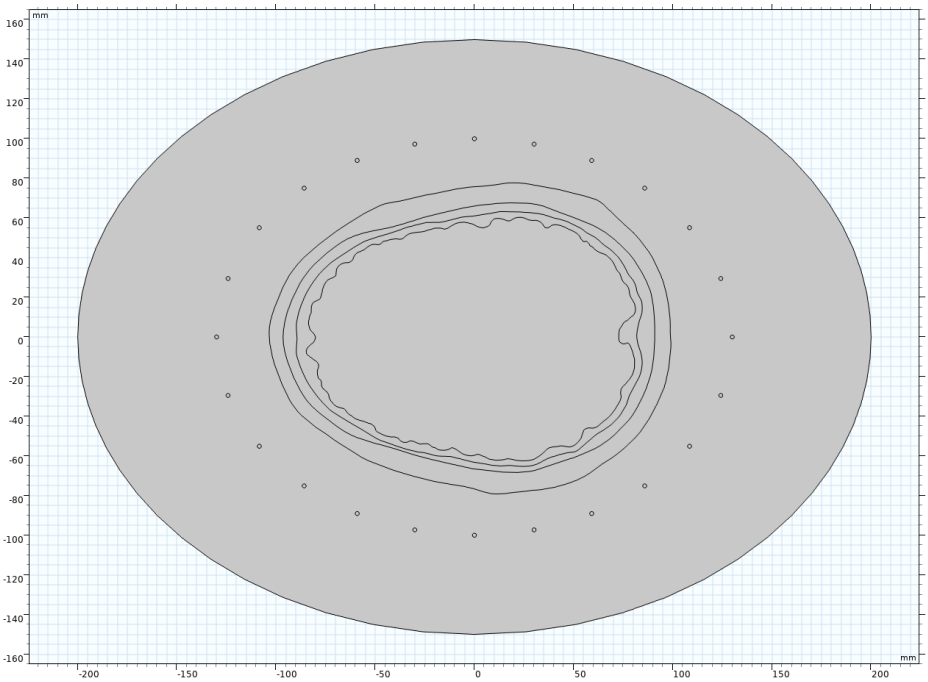

Figure 4.2: 2D slice of head with 24-antenna HT system

The distance between the single antenna elements varies with its number. I present these values in the *Table 4.1*. Knowledge of these dimensions is important for the next spatial arrangements of the designed antenna with the characteristics estimated from the simulations results.

Table 4.1: Distance between 2 neighbouring antenna elements for every HT system

Number of antennas	**24**	**16**	**12**	**8**
***Distance between two antennas* (mm)**	30	46	59	86

For correct simulation of human tissue, it was necessary to assign every layer its correct electromagnetic and physiological property based on the frequency used. These properties include relative permittivity, relative permeability, and electric conductivity. These values were obtained from the IT'IS Database for thermal and electromagnetic parameters of biological tissues. [19]

Table 4.2: Density and dielectric parameters of the head tissues used for the simulations. Dielectric parameters vary for each frequency. Data obtained from [19]

Tissue	*Density (*kg/m^3*)*	*Frequency (*MHz*)*	*Dielectric Parameters*	
			Electric conductivity (S/m)	Permittivity (-)
Scalp	1109	434	0.7	46.1
		650	0.78	43.1
		915	0.87	41.3
		1150	0.95	40.4
Skull	1908	434	0.09	13.1
		650	0.12	12.7
		915	0.15	12.4
		1150	0.18	12.2
CSF	1007	434	2.26	70.6
		650	2.32	69.3
		915	2.42	68.6
		1150	2.53	68.2
Brain tissue (GM+WM)	1046	434	1.05	55.1
		650	1.15	51.6
		915	1.27	49.3
		1150	1.38	48.1

Dielectric parameters can be as well implemented in COMSOL simulation using Cole-Cole models from MATLAB. These models include function for relative permittivity and conductivity based on the frequency used that can be directly imported into COMSOL parameter settings.

Physics

For the numerical simulation in COMSOL, the *Finite Element Method* was used to solve frequency domain form of Maxwell's equations. It is based on the discretisation of models, where a geometrical model is replaced by a finite number of elements. The physics problem is then calculated for every element separately, using method of numerical mathematics and the resulting distribution of fields is later estimated by combination of each element.

For calculation of SAR in the head model and further parameters involving its use, we need to obtain the distribution of electric fields (E-fields) in human tissue from the antenna applicator. The study chosen for computation of E-fields was the ***Electromagnetic Waves, Frequency domain***. This study is part of the Radiofrequency module in COMSOL. Whenever the solution of an electromagnetic field is wave-like, such as in radiating structures, or in other cases where the wavelength is comparable to the objects' sizes, the problem can be treated as a wave electromagnetic problem.

$$\nabla \times \mu_r^{-1} \cdot (\nabla \times E) - k_0^2 \cdot (\varepsilon_r - \frac{\mathrm{j} \cdot \sigma}{\varepsilon_0 \cdot \omega}) = 0 \qquad (4.1)$$

Where ∇ is the vector differential operator, μ_r is the relative permeability, E represents the electric field intensity in V/m, k_0 is the wave number of free space, defined as a ratio of angular frequency and the speed of light, ε_r is the relative permittivity, j is an imaginary unit of a complex number, σ is the electrical conductivity in S/m, ε_0 is the permittivity of the vacuum in F/m. [24]

In the physics setting, we must define *Initial* and *Boundary conditions*. The Initial conditions characterise the state of the model at the beginning. In our case it is at time t = 0 and the vector of the intensity of the electric field is set to zero. The boundary conditions are simulations of the interaction between the model and the outer world. In our case, *Scattering Boundary Conditi*on was used, which causes that chosen area to be transparent for the planar scattered wave and for other types of waves there is a perfect reflection of the boundary condition. The parameters are to be propagated from *Ports*, where the EM is generated. These are surrounded by *Perfect Electric Conductors* or *PEC*s.

4.3 Particle swarm optimisation

The distribution of electric fields in every tissue was exported into MATLAB for further optimisation of SAR delivery to the tissue. The aim of this optimisation was to minimalize hot spots in the healthy tissue and maximise the power delivery into the target area of the tumour. The imported data from COMSOL included matrices of electric field distribution for four chosen frequencies. Before optimisation, the ten positions of the target area were set and for each position, three sizes of tumours were created. To obtain correct results of power deposition in selected tissues, the dielectric parameters on chosen frequency and density of each layer were defined.

For optimisation, we have chosen the particle swarm algorithm, which has been proven to gain better results as a genetic algorithm. Particle swarm optimisation (PSO) is a population-based search algorithm. It was based on the phenomenon of bird movement within a flock resulting in an optimal formation after regrouping. The changes of single element, a particle, are affected by the knowledge of its neighbours. Therefore, a particle stochastically returns toward the regions of previous success in search space. The number of iterations was set to 200 for each case and the optimised parameters were phase and amplitude of every antenna for power steering of SAR delivery into the target.

SAR is calculated as:

$$SAR = \frac{\sigma \cdot |E|^2}{2 \cdot \rho}, \tag{4.2}$$

where σ is electric conductivity biological tissues in S/m, $|E|$ is a root mean square value of electric field strength in V/m and ρ is a density of the tissue in kg/m^3.

For the SAR indication, the Hotspot-to-Target Quotient (THQ) was used. THQ value expresses the ratio between the average SAR in hotspots, characterised as 1 % of the volume of healthy tissue where the greatest values of SAR are found, to the mean SAR in the target volume of our tumour. [25]

$$HTQ = \frac{SAR_{V1\%}}{SAR_{TARGET}} \tag{4.3}$$

Other SAR treatment quality indicators which are calculated from the SAR evaluation of PSO are the target coverage values (TC*X*). TC is defined as the percentage of Hyperthermia Treatment Volume (HTV) covered by 25 %, 50 %, and 75 % iso-SAR values. The distribution of SAR was normalised to the maximum SAR in the whole patients' head models. The level of target coverage was evaluated at 25 %, 50 %, and 75 %.

The aim of the optimisation is to:

1. Minimise the HTQ parameter
2. Maximise the tumour coverage (TC25, TC50, TC75)
3. Correctly cover the whole area of the tumour using power steering of antennas

4.4 Design of antenna element

We can characterise an antenna as any device which radiates electromagnetic energy for the purpose of power or signal transmission. One of the simplest constructions is the dipole antenna. It is realised using two metallic arms that have a sinusoidal voltage difference applied between them. The length of the arm is calculated using a quarter of the wavelength of the operating frequency. Dipoles are constructed in such way that the inner conductor of the coaxial cable is soldered on one arm while the outer conductor is soldered to the other. This minimises the impact of the coaxial cable on the radiating element.

The dipole antenna was chosen as the best approximation of the point source used in the 2D simulations.

In COMSOL software Finite Element Method was used to establish the correct dimensions of the dipole antenna to fulfil the requirements of the reflection coefficient of the antenna element based on its operating frequency advised from the results of simulations. For the given frequency, *Parametric Sweep* analysis is used to find ideal dimensions where the estimated frequency is also the resonant frequency of the antenna, and the return loss is at least -10 dB.

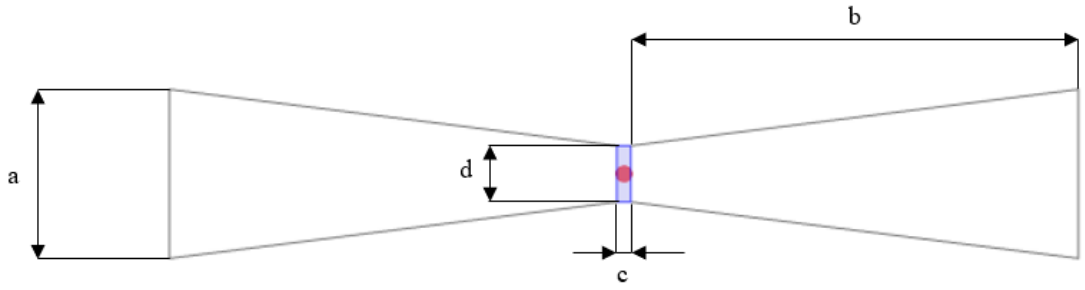

Figure 4.3: The parameters describing the dimensions of dipole antenna. Lumped port is marked with red dot between the arms of the antenna

4.4.1 COMSOL settings

As the result of the parametric study of antenna dimensions in COMSOL, the following sizes were chosen for the antenna manufacture:

Table 4.3: The values of antenna dimensions from Figure 4.3

Parameter	**a**	**b**	**c**	**d**
Size (mm)	12	31.75	1	4

First and foremost is the creation of *Geometry* model of the dipole antenna, water bolus, substrate in which the antenna is placed and block representing brain tissue parameters. The next step is to set the physical properties (*Materials*) of each area of the model. This means, in the hyperthermia system model, identifying the regions that correspond to the brain tissue and setting the values of the parameters that describe that tissue for calculations from the field of the spread of the electromagnetic field, such as relative permittivity ε_r (-) and electrical conductivity σ (S/m). Dielectric parameters used for the brain tissue model are written in *Table 4.4*.

Then we need to set the boundary conditions (*Electromagnetic Waves, Frequency Domain*), the core of the whole simulation. This means defining the areas in which electromagnetic field propagation calculations will take place. This is primarily a determination of the metal parts of the model (*Perfect Electric Conductor*), what parts will be good conductors for a given frequency of electromagnetic waves and will therefore be identified in the model as ideal electrical conductors. Furthermore, this involves setting the location of the electromagnetic wave generation (*Port*) and setting the area on which boundaries there will be a minimal reflection of the electromagnetic waves (*Scattering Boundary Conditions*). There are other predefined *Initial values* which determine the state of the model before the simulations are run, in the case of simulations from the electromagnetic field area it is an electric field intensity vector $\vec{E}$(x, y, z) = 0.

After the boundary conditions settings, a computational net (*Mesh*) is generated for the model, computed by the *Finite Element Method*. The method involves the discretisation of a continuous model into a specific, finite, number of elements. The parameters describing the distribution of the electric field are then calculated at the nodal points of these elements. It is possible to set the shapes and sizes of these elements so that the whole model is fully discretised and there are no areas where the model cannot be addressed. The minimum size of the mesh elements *s* (mm) is dependent on the

wavelength of the electromagnetic wave λ (m) spreading through the material (tissue, air, metal, etc.). For our dipole antenna, the size of the mesh elements was set to 0.02 mm.

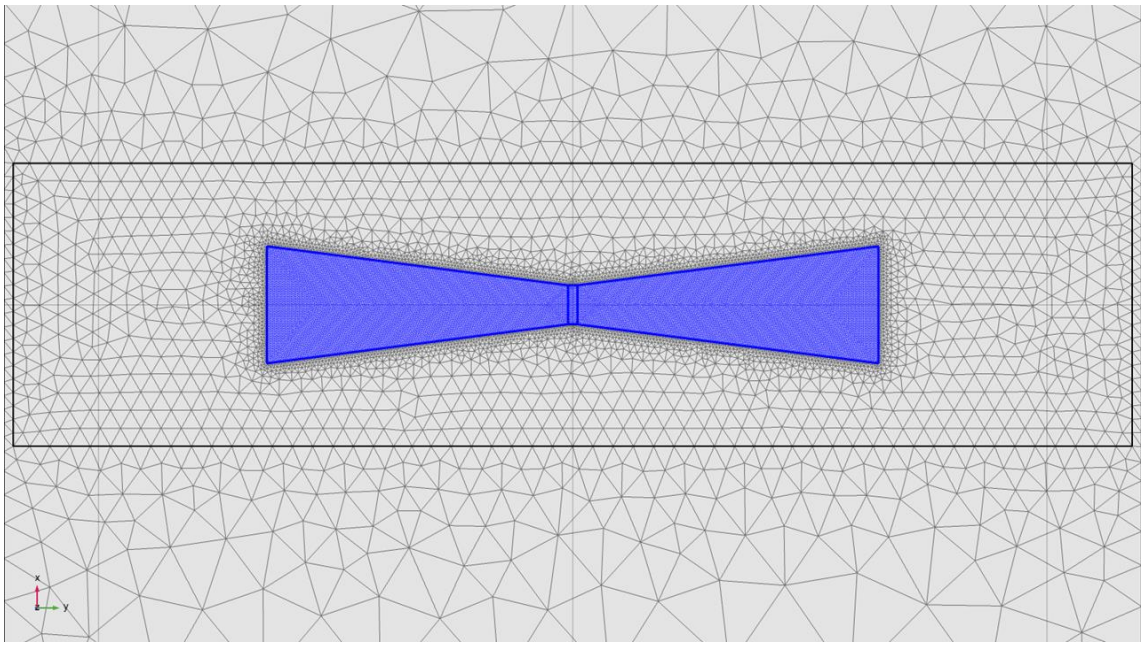

Figure 4.4: Mesh of the designed dipole antenna, size of the elements is set to 0.02 mm

Since the dipole antenna is very well known from other publications, e.g., [26; 27], mainly the interaction of this antenna with the biological tissue representing the head is mainly taken into account in this work. For this purpose, the calculated SAR value is compared with the measurement of this value on the cSAR 3D device. On the contrary, this information regarding the validation of the SAR quantity for one dipole is new compared to the mentioned works above.

For the manufacture of dipole antennas standard procedure was held using the etching of the antenna shape on a dielectric substrate, consisting of three layers. The base consists of a laminate (Cuprexit) made of glass cloth with epoxy resin. Next, there is a layer of copper on this laminate and the surface of the substrate is made of the photosensitive layer containing polymer. A dipole shape of our antenna was printed on transparent foil and applied to the substrate. Thus, the substrate was placed under UV light. Due to the UV radiation, the structure of the polymer contained in the photosensitive layer changes in every place except for the printed dipole shape. The plate is then immersed in a 1.5% aqueous NaOH solution. Sodium hydroxide causes the polymer to separate at the sites where the changing of its structure occurred. In the last step, the substrate is immersed in a bath of concentrated ferric chloride, which etches the copper layer from the substrate in places where the photosensitive layer has been removed.

A dipole antenna combined with balun (balanced-to-unbalanced transition) is reported to have a better response than a conventional dipole [28]. This element consists of a microstrip line grounded to one arm of the dipole located on the other side of the

epoxy substrate and acts aan a RF-matching network, which means it ensures a symmetric radiation field with stable electrical performance throughout whole frequency band [29]. The negatives of the antenna design with a balun, apart from adding complexity, is the necessity of enlarging the dimensions and decreased efficiency due to power absorption in the structure [30].

If we want to ensure the majority of the power of the EM wave is delivered, we must set all circuits, through which an EM wave is propagated to the same impedance. For an EM wave propagating with characteristic impedance, $Z_0 = 50\ \Omega$, the dipole antenna in its medium represents a load of impedance Z_L. Designing an antenna involves an approximation of Z_0 to Z_L. That way a power loss is minimised.

The dielectric parameters of the block which represents the phantom of the human head were set as follows:

Table 4.4: Dielectric parameters set in the COMSOL design of the antenna

Dielectric parameters of human head phantom [31]	
Electric conductivity σ(S/m)	Relative permittivity μ(-)
0.87	43.5

The parameter which will be computed is called reflection coefficient $|S_{11}|$ and represents how much power is reflected from the antenna. When a complex electromagnetic wave a_1 (V) of a certain amplitude and phase hits a port, part of this wave is reflected back as b_1 (V). The parameter is measured as a reflected signal of a signal injected at the port. The ratio of these two waves is represented by the S_{11} parameter (unitless), the so-called reflection coefficient, calculated as:

$$S_{11} = \frac{b_1}{a_1} \tag{4.4}$$

4.5 Measurement of SAR distribution in cSAR 3D head phantom

The most important requirement for the antenna set for medical application is the effectiveness of its radiation in an estimated frequency range. For the indication of the distribution of electromagnetic energy in human tissue, a specific absorption rate is measured. Other indirect techniques include the temperature measurements after the phantom heating or the electromagnetic field intensity measurements.

For the measurement of the Specific Absorption Rate of the designed antenna element, SAR System with Novel Vector Array Technology is used, called cSAR 3D developed by Swiss SPEAG. This system is used to evaluate wireless devices operating on a frequency range from 300 MHz to 6 GHz, it provides high-precision SAR measurements as required by IEEE standards. Each measurement takes less than 0.3 s for acquisition, post-processing and display. The system is filled with a broadband head simulating medium with the conformity of target dielectric parameters of less than 10 % across the whole frequency range.

Our dipole antenna was connected to the power generator operating at the frequency of 434 MHz. The power set on the generator was 140 W. An attenuator reducing power of the signal by 30 dB (a thousand times reduced power) was connected to the generator through coaxial cable. Therefore, the input power of the measured antenna was 0.14 W. This power value was set in the simulation settings as well. The outcome of the laboratory measurement in the phantom is the 3D map of SAR distribution in the tissue from the designed antenna which is placed on the surface of cSAR 3D.

5 Results

5.1 Electric field distribution in COMSOL

Solutions of the *Electromagnetic Wave, Frequency domain* study were represented by a surface colourmap or a matrix of values of electric field strength. As an EM wave propagates through different types of tissue with various scattering coefficients, the resulting map differs in magnitude at every layer of the human head model based on the frequency at which the EM wave travels. The matrices were imported to MATLAB where the amplitude and phase of each radiating element were optimised for the best coverage of the target volume set in the code.

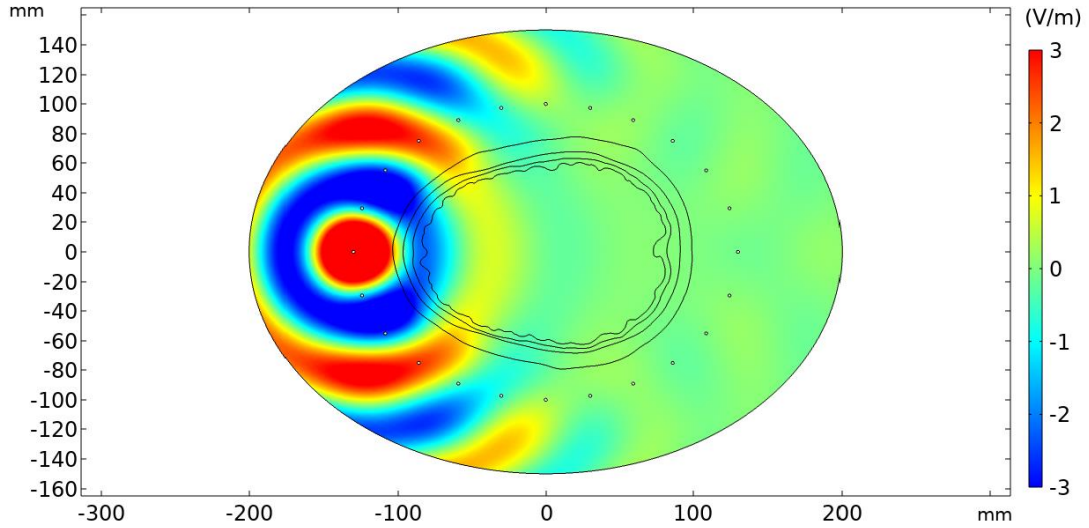

Figure 5.1: Distribution of electric fields in the HT system operating at frequency 434 MHz obtained in COMSOL

5.2 Results of PS Optimisation

In total, 4800 simulations were held differing in:

- Frequency (434 MHz, 650 MHz, 915 MHz, 1,150 MHz)
- Patient model (10 anatomical structures)
- Location of the target area (10 positions based on the most frequent occurrences of brain tumours)
- Size of the target area (20 mm, 25 mm, 30 mm)
- Number of antennas used for the simulation of the HT system (24, 16, 12 and 8 antenna system)

In the following chapters, I present the effect of each mentioned factor on the set of pictures depicting the distribution of SAR in the 2D slice of the head. As not only pictures but also quality parameters were obtained from the MATLAB simulation, each of the

examined parameters is graphically represented using the HTQ function and Target Coverage values.

5.2.1 Effect of Frequency Used

Four frequencies based on the most common hyperthermia application devices were compared, 434, 650, 915 and 1,150 MHz. The results were quantified with SAR quality statistics over the tumour volume with the TC25, TC50 and TC75 values, which show the fraction of the target area enclosed in the 25 %, 50 %, and 75 % isolines of peak SAR, respectively.

The target region in the pictures is delineated with a thin black contour. The following plot depicts the SAR distribution of 24 radiating antennas in the head of Patient 1 with the tumour located in the frontal lobe, 4 cm under the outer layer of the head model. The 24-antenna model was used as a representative figure, as the results obtained from this system show the greatest variances. The set of figures comparing frequencies of the remaining antenna systems are part of *Appendix A.*

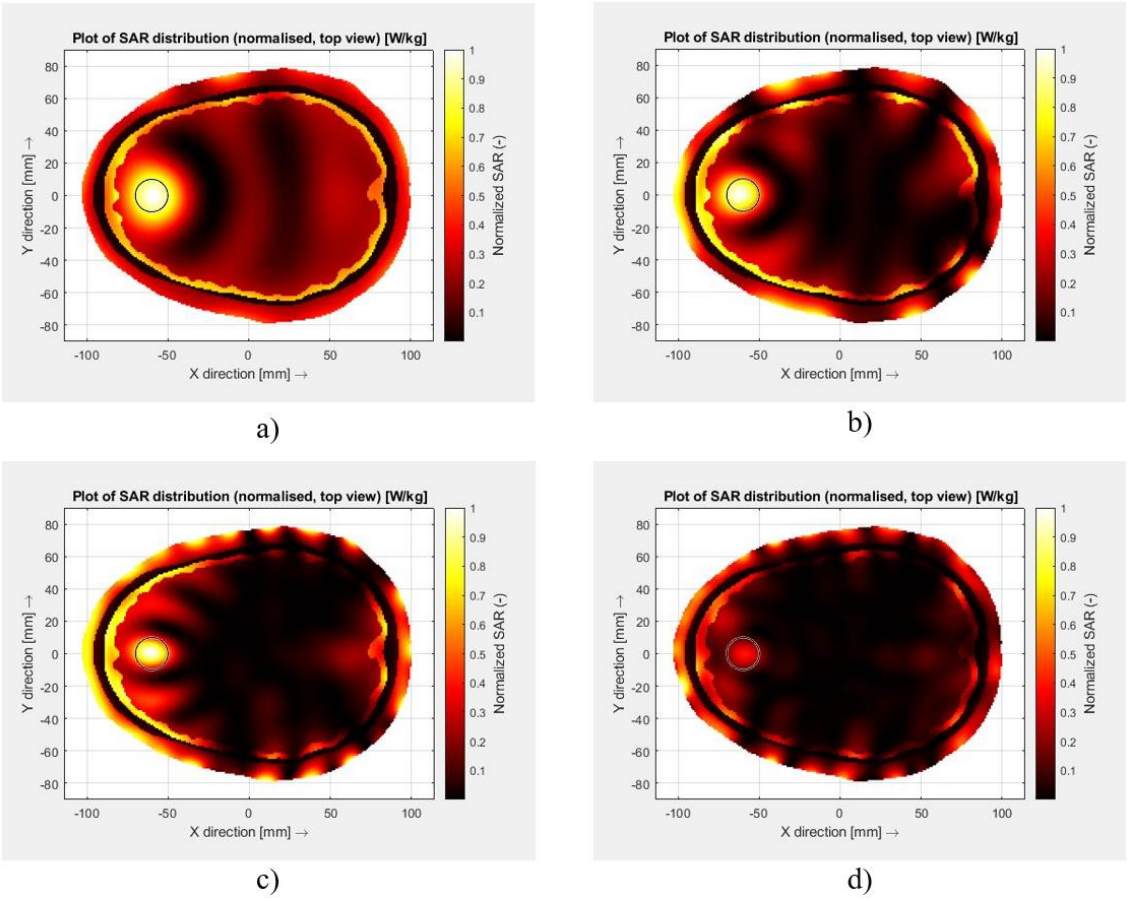

Figure 5.2: SAR distribution in the 2D head model obtained by a 24-antenna HT system on the frequency of a) 434 MHz, b) 650 MHz, c) 915 MHz and d) 1150 MHz

The following box plot shows the mean values of target coverage of 25 % of tumour volume by the highest SAR depositions. Minimum and maximum values are displayed by the tails of the graph while the box shows the interquartile range with the median (horizontal line) and mean (cross) values inside it. Values are averaged for 300 samples, made of data from 10 patients, 10 target locations and 3 sizes of the target.

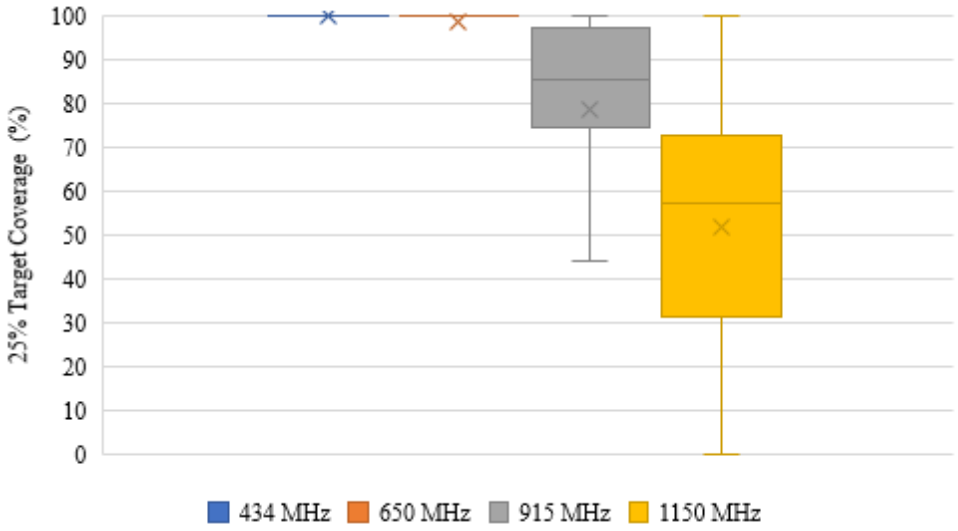

Figure 5.3: Box plot of TC25 comparing four frequencies used for a 24-antenna HT system. Mean values are represented by a cross

The box plots are used to compare the remaining percentages of tumour coverages. Again, the graphs depict values for the 24-antenna hyperthermia system. The 16, 12 and 8-antenna systems are graphically presented as part of *Appendix B*.

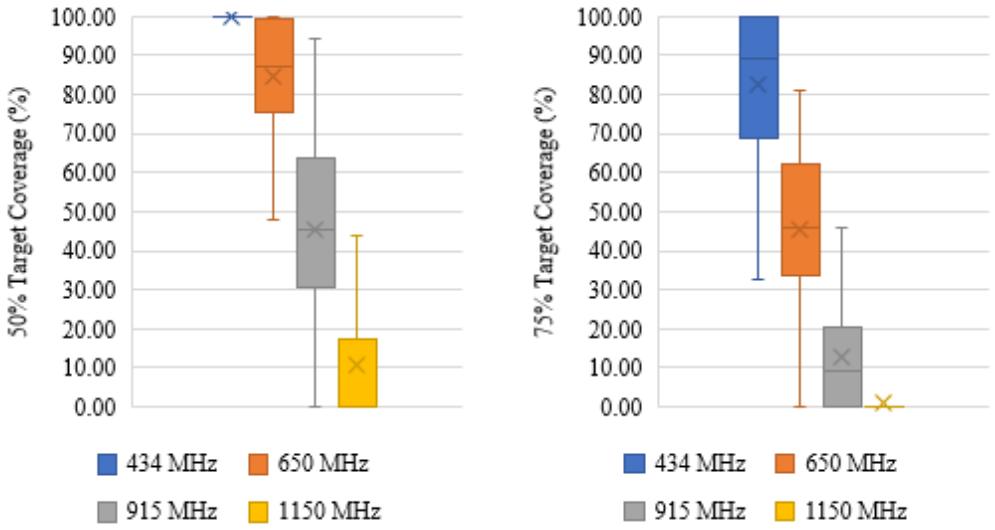

Figure 5.4: Box plot of TC50 & TC75 comparing four frequencies used for a 24-antenna HT system. Mean values are represented by a cross.

For a better comparison of exact values, the following table shows the mean values of treatment planning parameters with a range of minimum and maximum values of each target coverage by a 24, 16, 12 and 8-antenna system.

Table 5.1: Average values of TC25, TC50 & TC75 and the range of all its corresponding values for a 24antenna and 16antenna HT system

	Frequency (MHz)	***Target Coverage*** (%)			
		24-antenna system	*16-antenna system*	*12-antenna system*	*8-antenna system*
TC25	434	**100**	100 (99.57–100)	100 (99.57–100)	97.4 (3.89–100)
	650	98.6 (43.33–100)	**99.32** (80.49–100)	83.8 (0–100)	34.28 (0–97.70)
	915	**78.56** (0–100)	41.48 (0–100)	11.83 (0–85.57)	0 (0–0.66)
	1150	**51.76** (0–100)	1.69 (0–100)	0	0 (0–0.29)
TC50	434	**99.76** (85.5–100)	99.79 (75.32–100)	99.22 (55.67–100)	19.55 (0–100)
	650	84.61 (0–100)	**86.45** (20.25–100)	21.59 (0–100)	0
	915	**45.61** (0–94.43)	1.76 (0–50.49)	0	0
	1150	**10.99** (0–77.05)	0	0	0
TC75	434	82.54 (0–100)	**82.71** (0–100)	75.87 (0–100)	0
	650	**45.53** (0–80.98)	42.74 (0–84.59)	0.45 (0–28.2)	0
	915	**12.89** (0–45.90)	0	0	0
	1150	**1.178** (0–37.38)	0	0	0

The analysis obtained from the graph shows us that the highest values of target coverage are reached by the 24 and 16-antenna HT system operating on the frequency of 434 MHz (bolt). Since a smaller number of antennas is more advantageous both in terms of finance and construction, the 16-antenna HT system is preferred over the 24-element one.

Another examined quality parameter for the study of the frequency impact is the Hotspot-to-target quotient, representing a balance of power deposited within and outside of the hyperthermia treated volume. *Table 5.2* reports the results for all 4800 simulations computed with the mean value of the quotient and the standard deviation of all the values accounted for.

Table 5.2: Mean values and standard deviations of HTQ for 4 used frequencies of every HT system

HTQ	*Frequency* (MHz)			
Number of antennas	***434***	***650***	***915***	***1150***
24	**0.88±0.11**	1.06±0.28	2.27±2.59	3.78±4.18
16	0.89±0.11	1.13±0.18	2.91±1.25	6.08±3.88
12	0.96±0.14	1.91±0.65	5.69±6.26	8.25±3.96
8	1.78±0.41	3.13±1.13	6.07±2.12	10.22±5.18

For an illustrative comparison of HTQ, I present the following bar graph showing the increase of the quotient depending on the number of radiating antennas and the frequency of antennas. It is visible that in every case the quotient increases with increasing frequency and with decreasing number of radiating antennas.

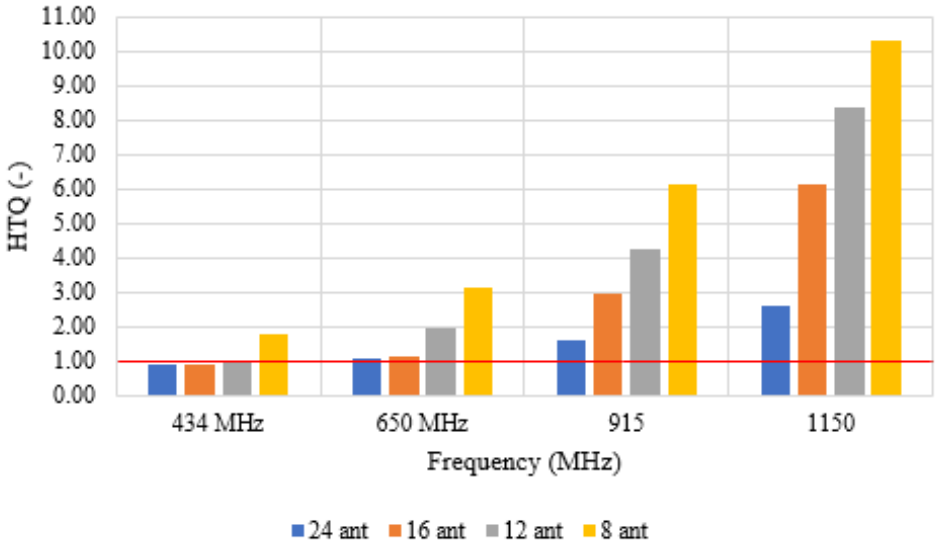

Figure 5.5: Hotspot-to-Target Quotient based on the varying frequency and number of antennas used for HT treatment. The red line shows the ideal maximum value of HTQ

Effect of number of antennas used

Part of the analysis was to determine and compare the number of antennas used for the whole-tumour coverage. Logically, increasing the number of radiating bodies also increases the energy delivery to the tissue. This may be at the expense of unwanted hot spots created in healthy tissue. As the effort is to build an affordable hyperthermia system, the aim is to establish how much of the SAR would be reduced, decreasing the number of antennas.

Based on the results from the previous frequency analysis, the frequencies 915 MHz and 1150 MHz show minimum tumour coverage by isoSAR, that is why for the analysis of the antenna count I use the two lowest frequencies.

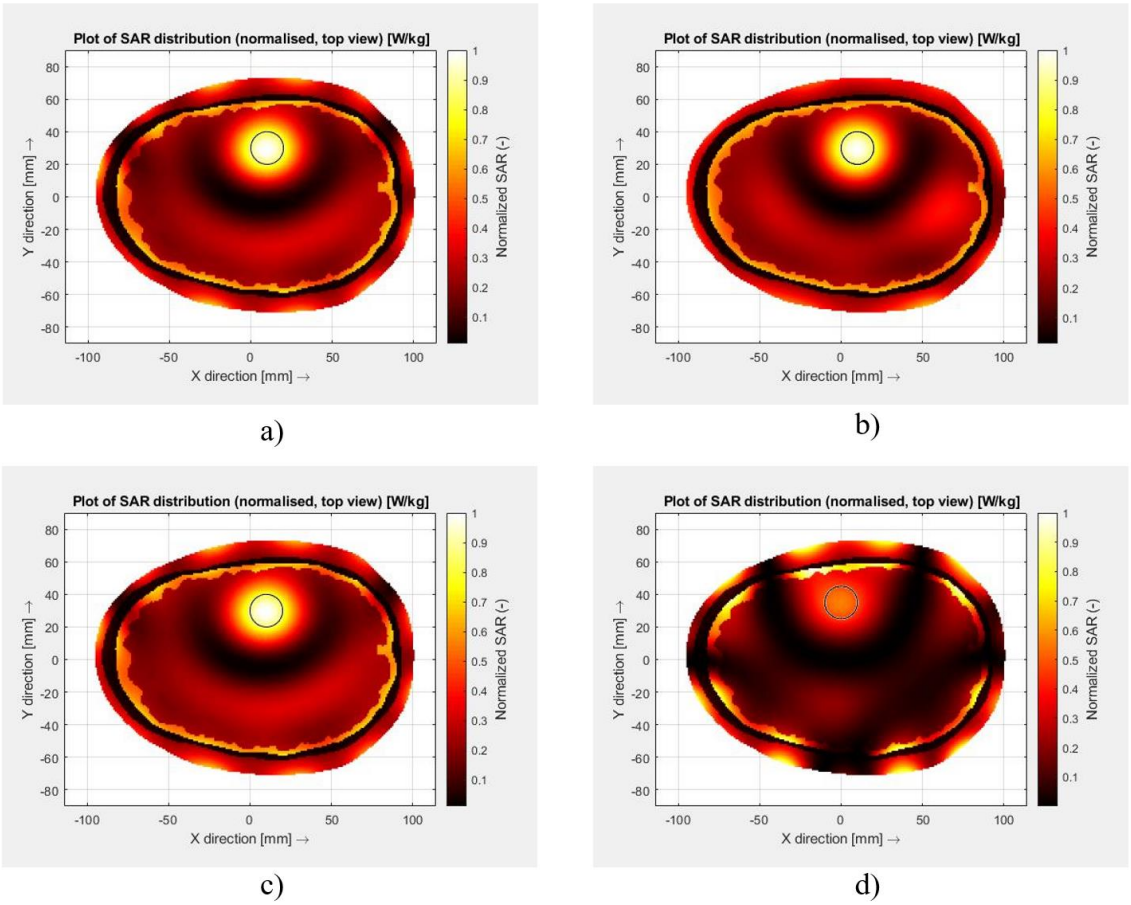

Figure 5.6: SAR distribution in the 2 D head model obtained by a) 24-antenna, b) 16-antenna, c)12 antenna and d) 8-antenna HT system on the frequency 434 MHz

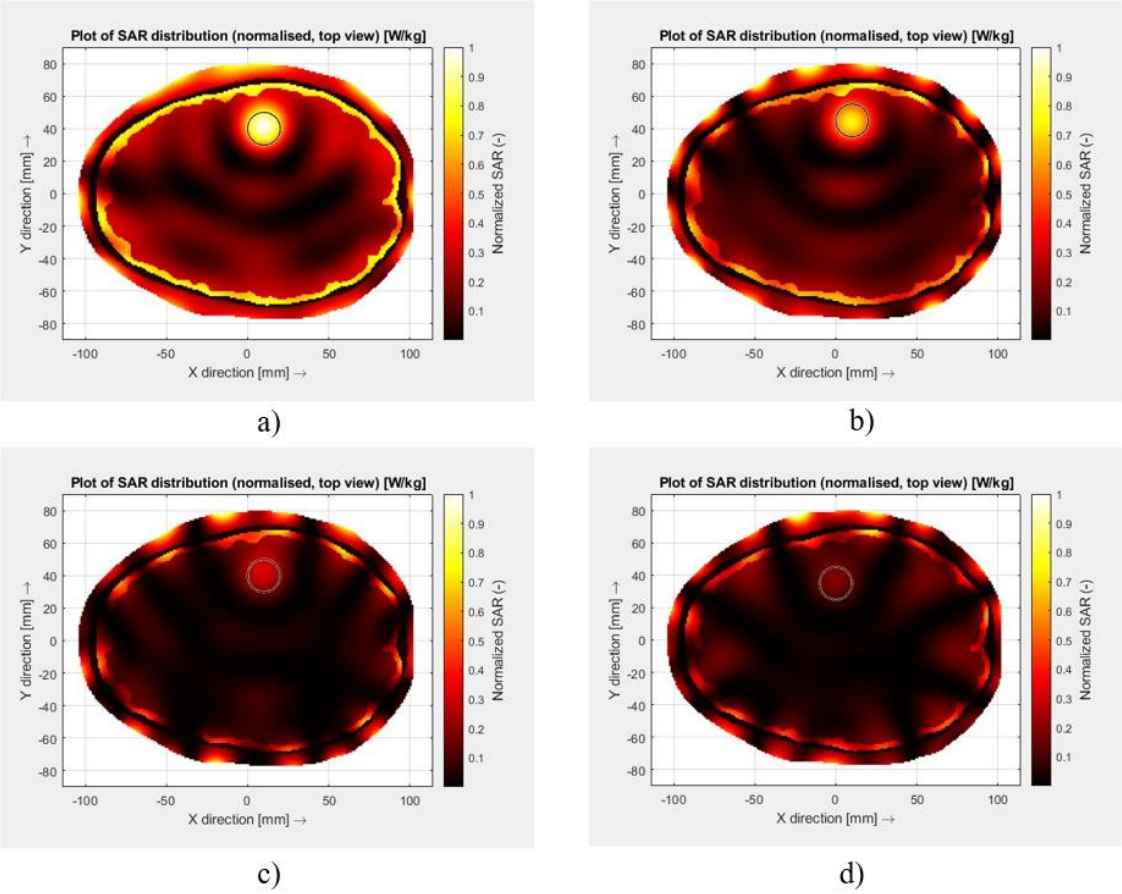

Figure 5.7: SAR distribution in the 2D head model obtained by a) 24-antenna, b) 16-antenna, c)12 antenna and d) 8-antenna HT system on the frequency 650 MHz

For the comparison of target coverage, the following bar graph shows the mean values of TCs for every antenna arrangement. Graph showing the comparison for every frequency is part of *Appendix C.*

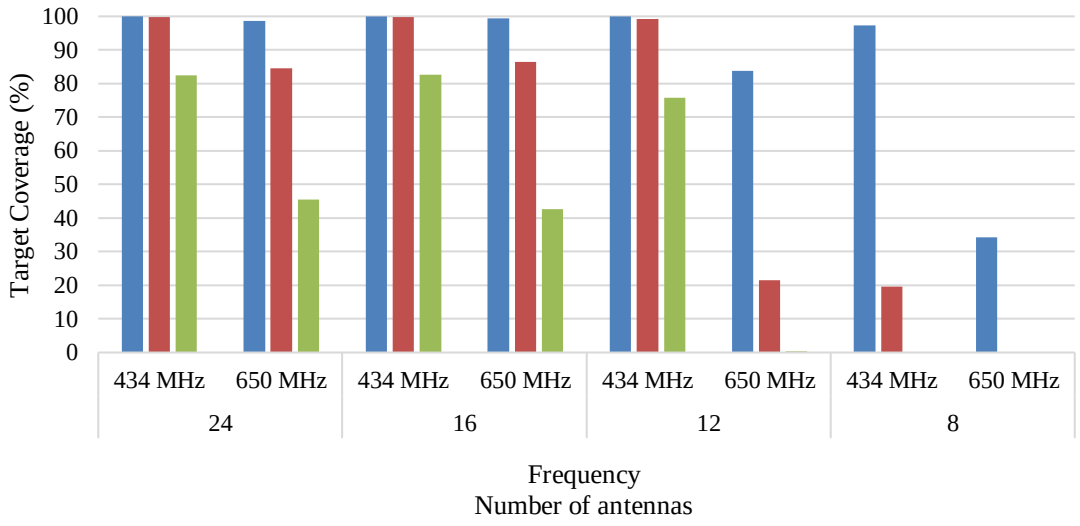

Figure 5.8: Target Coverage comparison for four antenna number of the HT system operating at the frequencies 434 MHz and 650 MHz

5.2.2 Effect of tumour size

The application system should heat the entire target volume. To obtain full coverage of the tumour, multiple abutting fields should be outlined. That is why not only frequency, but the number of radiating elements should be considered in the analysis.

The next 2 figures analyse how the 24-antenna system operating on a frequency of 434 MHz & 650 MHz covers 3 different sizes of target area enclosed inside the black circle.

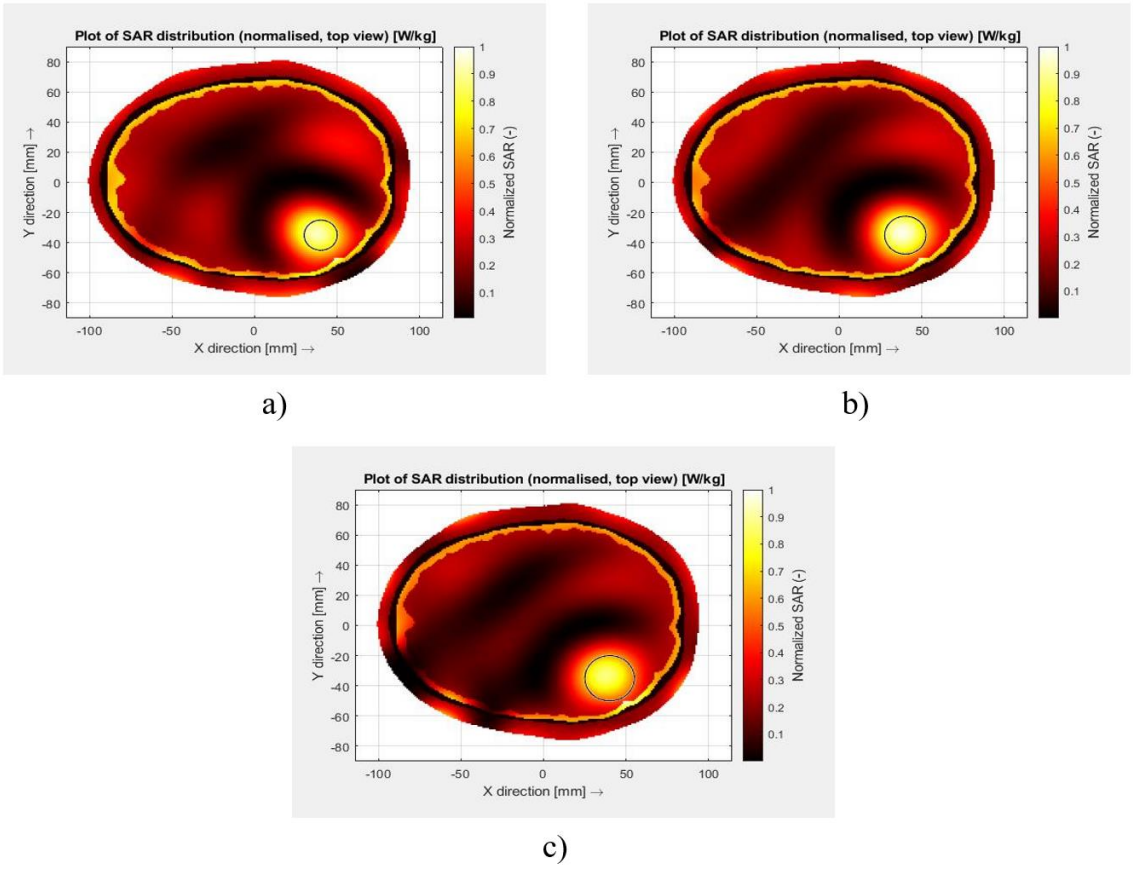

Figure 5.9: SAR distribution of 24-antenna HT system on the 434MHz frequency for three sizes of tumours a) 20 mm, b) 25 mm, c) 30 mm

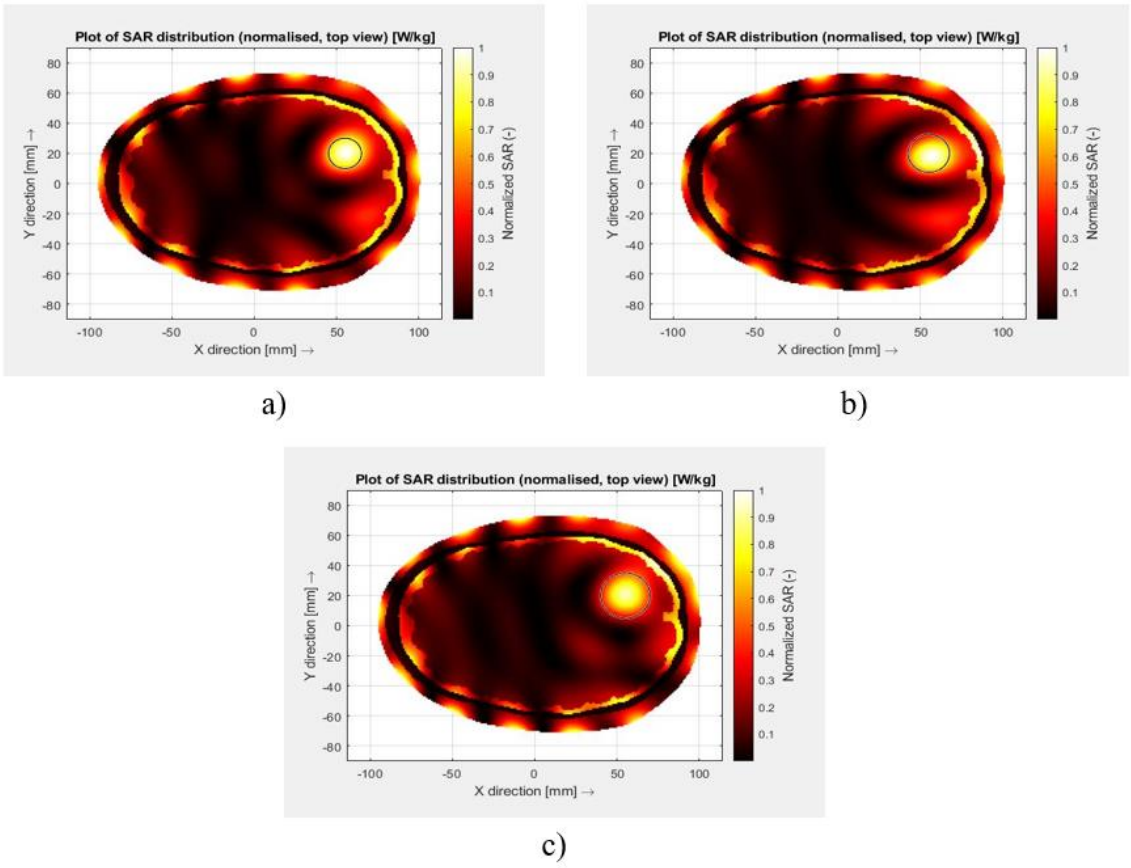

Figure 5.10: SAR distribution of 24-antenna HT system on the 650MHz frequency for three sizes of tumours a) 20 mm, b) 25 mm, c) 30 mm

The influence of the number of antennas on the coverage of tumours with different diameters is shown in *Figure 5.10* for two frequencies of the highest impact.

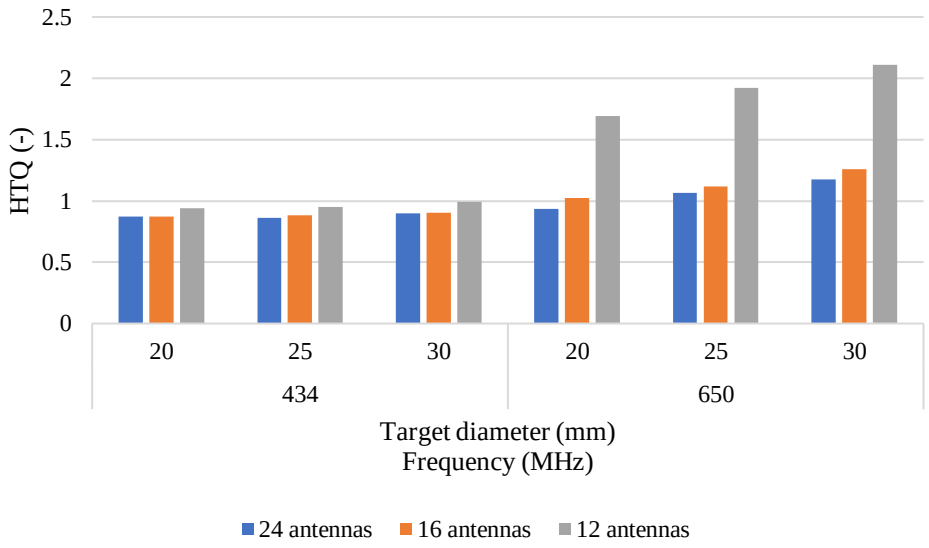

Figure 5.11: Comparison of HTQ in 3 different sizes of target areas for two lowest frequencies of 24, 16 & 12 antenna system

HTQ value for every size of target area remains under the critical value of 1 for 24, 16 and 12 antenna systems operating at frequency 434 MHz.

For comparison with other operating frequencies, I present the following graph, which contrasts the HTQ in three sizes of the target volume for the 24-antenna system.

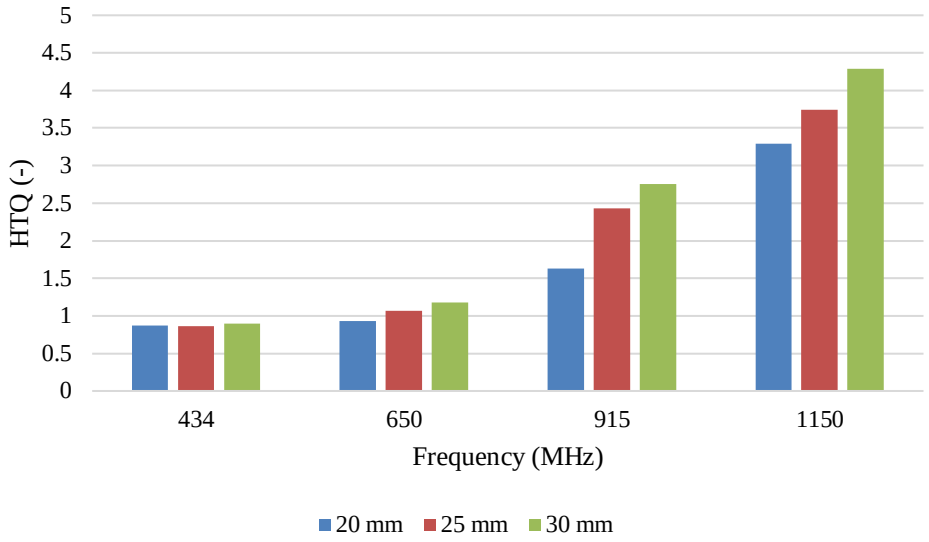

Figure 5.12: HTQ in the three sizes of target area compared with increasing frequency of the 24-antenna operating system

From *Figure 5.11*, we can summarise that even the highest antenna number of the HT system operating at the frequency of 650 MHz does not keep the value of HTQ under 1 in the two largest target areas.

5.2.3 Effect of tumour location

For the most frequent locations of head tumours, the frequency and antenna count analysis was held. Tumours placed in the three most recurrent lobes, frontal, temporal, and occipital were in approximately the same depth while on the contrary, the tumours in the central part of the brain were located from 8 to10 cm beneath the skin.

Figure 5.12 compares the HTQ of various tumour locations for four different frequencies of the 24-antenna system.

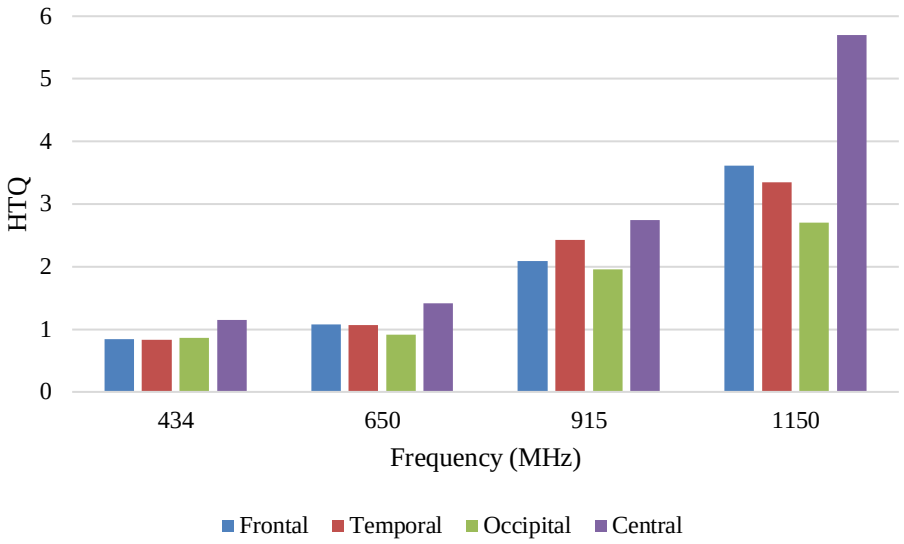

Figure 5.73: HTQ for the tumours located in the frontal, temporal, occipital and central part of the brain differing in the frequency of 24-antenna system

While the target area located in the central part has the highest hotspot ratio for every frequency used, specific lobes of the brain seem to have no significant difference in the resulting quality of HT treatment.

From the previous analyses, it is obvious that the lowest frequency offers the best results from every analysed parameter. The following graph compares the HTQ value at the chosen target locations for all HT systems operating at the frequency of 434 MHz.

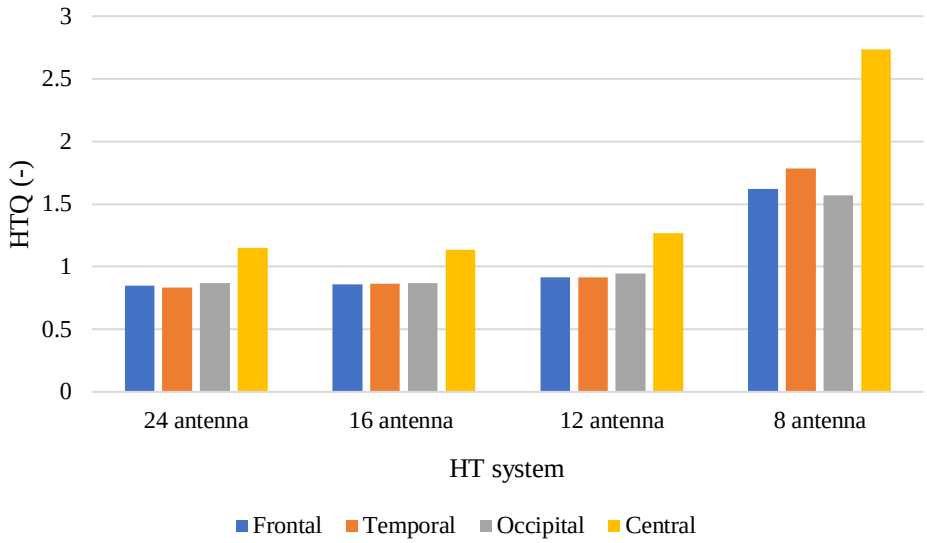

Figure 5.84: HTQ for the tumours located in the frontal, temporal, occipital and central part of the brain, differing in the number of antennas used for the HT system

Figure 5.13 confirms the presumption that the HT systems of at least 12 antenna elements operating at the frequency of 434 MHz are capable of delivering wanted power to the tumours located on the outer margin of the brain without depositing the majority of SAR in undesired hotspots.

The figure on the following page depicts the SAR distribution in ten locations of the target areas.

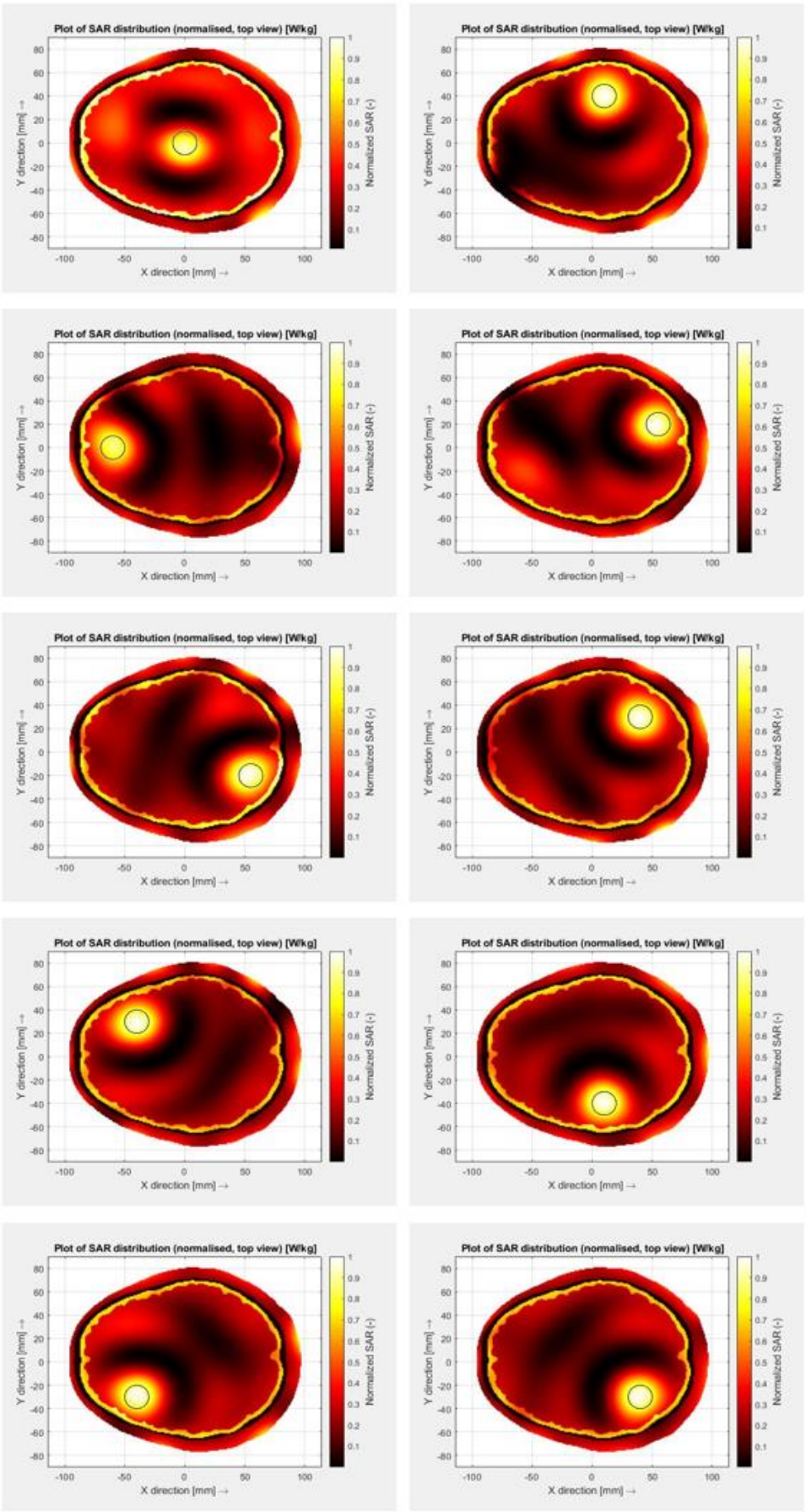

Figure 5.15: Comparison of SAR distribution in 10 different locations of target area

5.2.4 Antenna amplitude distribution

The results of the particle swarm optimisation were adequate settings of phase and amplitude of every antenna used in the array. An interesting point of the analysis is knowing how the power steering works based on the computed amplitudes.

The following radar graph depicts the amplitudes of twelve radiating antennas used to heat the tumour in the frontal lobe of the brain (located at the proximity of antenna number 10).

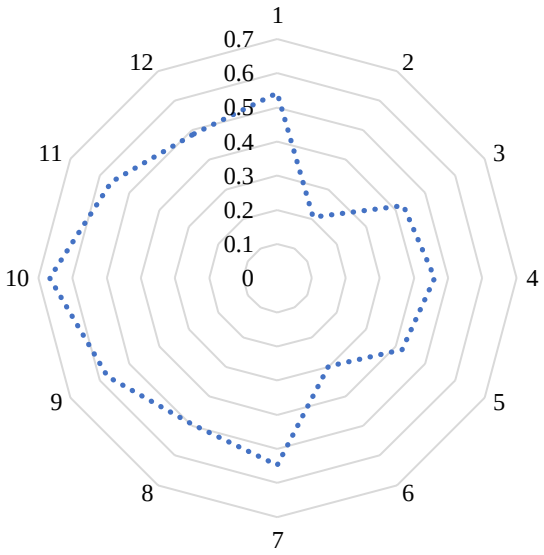

Figure 5.96: Radar graph showing the amplitudes of 12 antennas focusing on the tumour in the frontal lobe (located at the proximity of antenna 10)

The power steering used by the optimisation results in an amplitude increase of the antennas that are located at the shortest distance from the target.

5.3 Antenna design and measurement

Based on the simulation results described above, the frequency of 434 MHz was chosen for the antenna design. In Figure 5.17 the current density in the dipole antenna is zoomed.

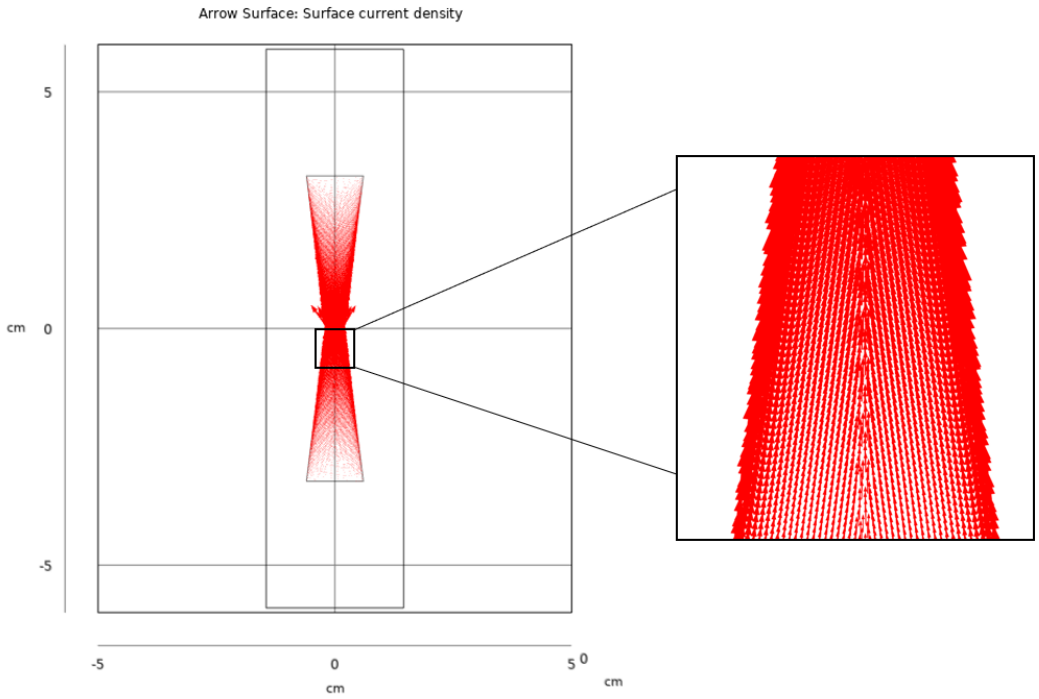

Figure 5.107: Dipole antenna design and its current density distribution

For these antenna parameters, the scattering coefficient does fulfil the requirement of the return loss of less than -10 dB as is shown in the next figure

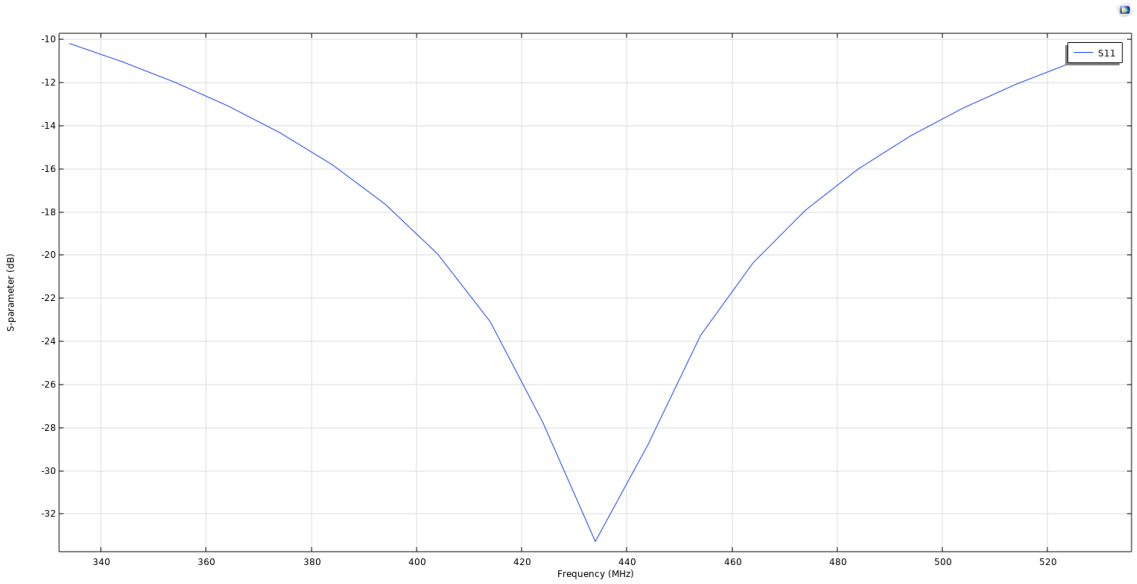

Figure 5.118: S11 parameter of the antenna at the frequency of 434 MHz

During manufacture, the balun element intended to be part of the dipole during simulation steps, was avoided due to the obtuse soldering between the arms of the dipole. Adding this complexity to the designed element would require change of the dimensions. However, avoiding the balun increases the efficiency due to the power absorption in the structure and moreover ensures the EM combability.

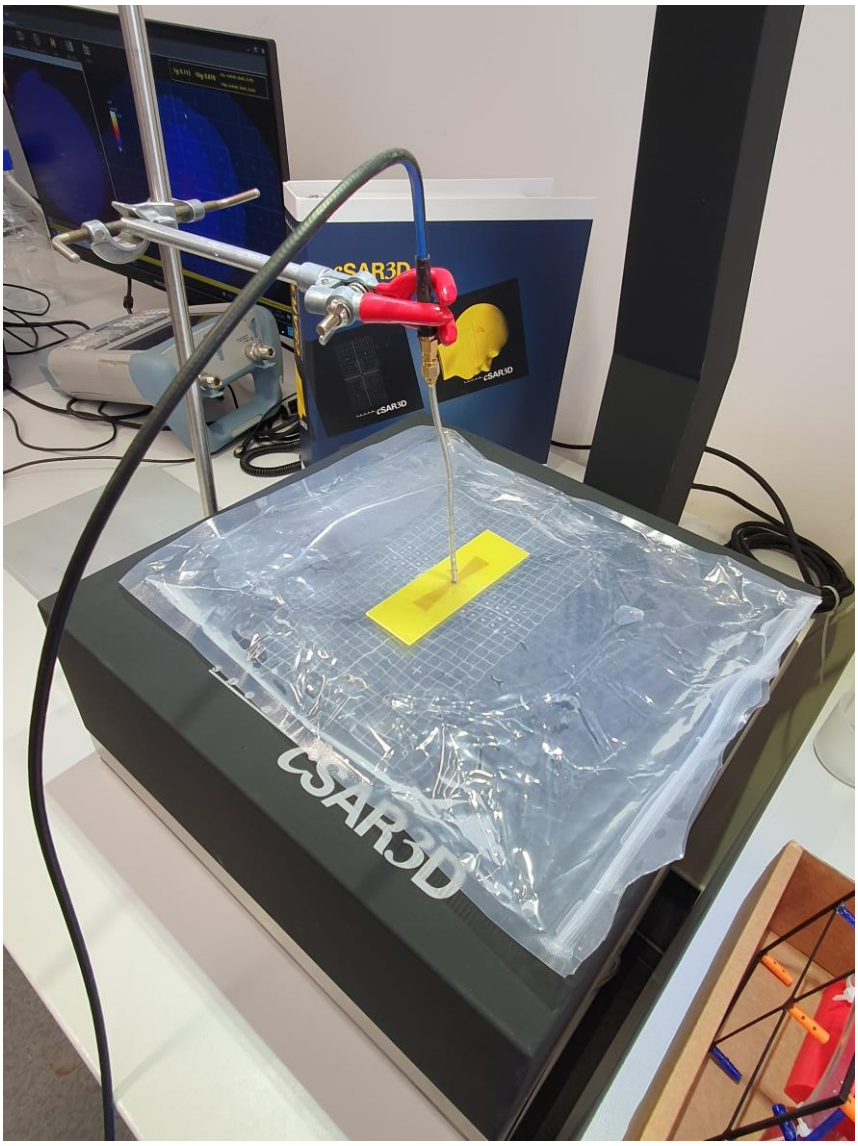

Figure 5.129: Positioning the designet dipole antenna on the cSAR 3D phantom. Between the phantom and dipole, a water bolus is placed for coupling of the EM energy

5.4 Measurement of the designed antenna

The measured parameter S_{11} met the estimated criterion of delivering power loss of -11 dB at the frequency of 434 MHz.

The SAR distribution obtained from the cSAR3D head phantom is depicted in the next figure. For comparison of simulations and experiment, I present the SAR distribution in head phantom on the left side and SAR value perpendicular to the centre of the dipole in COMSOL simulations on the right

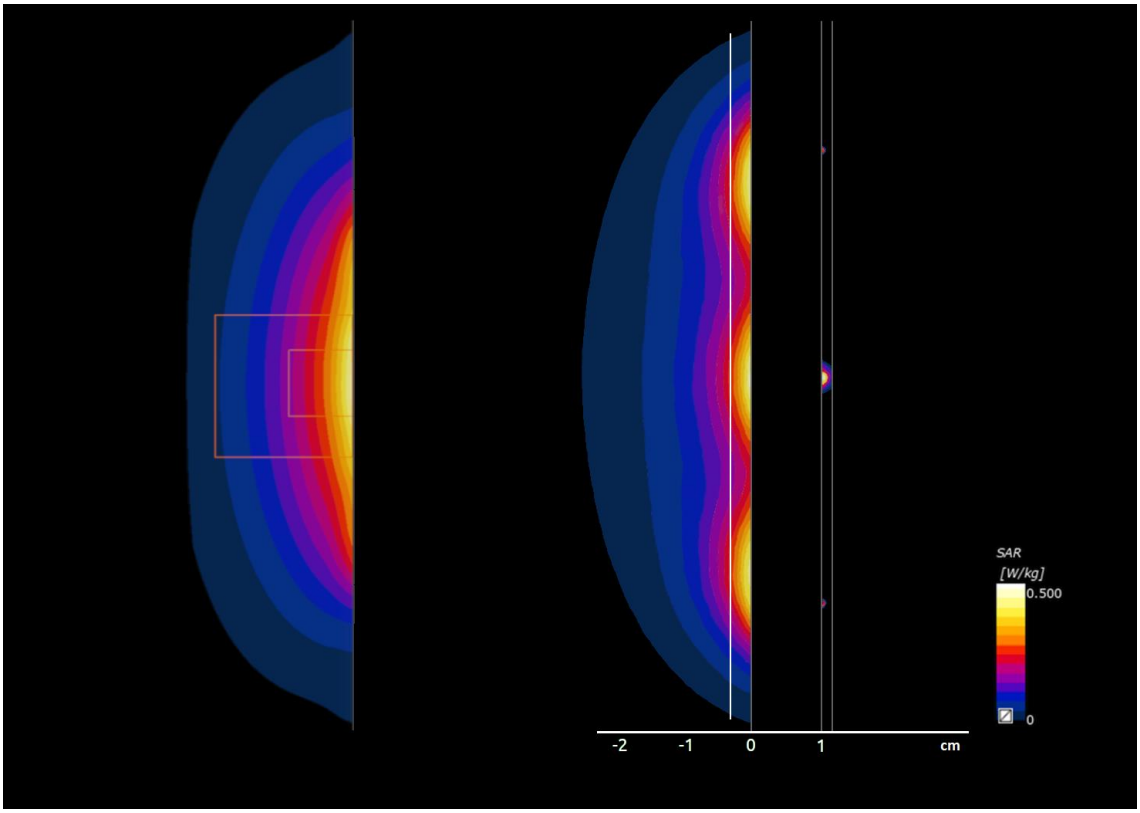

Figure 5.20: Comparison of the SAR distribution in head phantom measured experimentally (left) and SAR distribution of designed antenna in COMSOL (right)

In the SAR distribution from COMSOL simulations (right), the white vertical line in 3 mm is added to correctly scale the radiation pattern to the SAR distribution in phantom model (left), which also begins in 3 mm depth of the tissue.

6 Discussion

The simulation set-ups of 4800 possible scenarios of HT treatment were considered for the analysis of ideal operating frequency and number of radiating antennas of the hyperthermic system. Ten segmented patient head models with different anatomical structures were used, as even small difference in the structure of brain can result in different outcome of the treatment (volume of CSF, thickness of the skull, head shape) [32]. Targets were positioned in 10 different locations of the brain tissue, all around the 5cm rim of the brain tissue. One target was located in the centre of brain for determining the effective depth of treatment. The size of the target was 20, 25 and 30 mm for every location. The results were evaluated using the recommended guidelines of quality parameters of hyperthermic systems, which are standardised and regularly updated by ESHO. The optimised parameters were the tumour coverage or areas enclosed by the 25%, 50% and 75% iso-SAR contours. The object of the optimisation was to maximise these parameters while on the other hand, the Hotspot-to-Target Quotient was minimised. The latter describes how much power is delivered into the healthy tissue compared to the power delivery in the chosen target. Reasonably, this value is ideally below 1. The localisation of the target was programmed by finding the best values of amplitude and phase of each used antenna, in a so-called power steering. This is system is frequently used in commercially built hyperthermic systems. For visualisation how the SAR is distributed in the 2D head model, the figures presented in the Results are depicting how the frequency and antenna number influences the pattern of SAR in the tissue. The highest amount of unwanted SAR is deposited in the cerebrospinal fluid, because of its dielectric characteristics, high permittivity, and conductivity. The skull, with lower values of dielectric parameters has the lowest amount of SAR deposited in its tissue. In real patient models, parameters that lower the expected heat delivery into head tissue should be considered. These parameters are the volume of CSF, as by its circulation the cooling by convection occurs. Other cooling conditions are respiration, evaporation and sweating, as well as the metabolism of an individual.

Taking into account all the simulation results I conclude the following statements concerning the hyperthermia treatment of brain tumours:

1. *The ideal frequency for antenna element is 434 MHz*

From the initial analysis of the frequency effect, it follows that with increasing frequency, the coverage of the target area decreases and the distribution of SAR in the unwanted areas appears (*Figure 5.5*, *Table 5.1* & *Table 5.2*). Compared with other higher frequencies 650 MHz, 915 MHz and 1150 MHz, the chosen frequency of 434 MHz was capable of delivering the majority of the total SAR into the target area in every scenario. This confirms the known fact that lower frequency electromagnetic waves penetrate

better with anatomical structures than short-wavelength EM waves, although for more complex tumour shape, a larger wavelength (3–4 cm) could cause damage to the surrounding healthy tissue. Our result also verified the effectiveness of hyperthermic systems used in Europe operating on this frequency, such as HYPER collar [33] or Alba ON 4000 [34].

2. *Twelve antennas are the optimal number for the HT phased array system*

Compared with two higher antenna numbers (24 & 16) and one lower (8), the 12 antenna HT system, operating on the frequency of 434 MHz, fulfilled the requirements of minimising the HTQ parameter below the critical value of one while keeping the target coverage to a maximum percentage *(Figure 5.5* & *Figure 5.8*). As expected, increasing the number of radiating elements results in higher SAR deposition in the tissue. This trend can be seen in *Figures 5.6* and *5.7*, comparing the frequencies of 434 and 650 MHz. However, considering the financial and manufacturing approach of the system, finding the least number of antennas capable of delivering the required heat to the treated area is the aim of current studies. In my work, I contradict the study [35], where 8 antennas operating on the frequency 434 MHz were sufficient in delivering the heat to head & neck tumours. The result of this analysis inclines towards the study [36], where the minimum number of 12 antennas was recommended.

3. *The chosen combination of 434 MHz and 12 antennas is recommended for the clinical trials of heating head tumours of size up to 30 mm, situated in the 5cm depth of the head tissue.*

By analysing the success rate of treatment for the various tumour occurrence, we can summarize that the result of treatment depends on the depth of the tumour laid rather than its specific area in the head. While for targets, occurring at a depth of up to 7 cm below the surface, not even a 24-antenna HT system is sufficient, for additional targets located less than 4 to 5 cm below the surface of the scalp the 24, 16 and 8 antenna HT system operating at the frequency 434 MHz met the requests for SAR coverage of the 3 frequently recurring brain tumour locations.

The next part of this thesis was the design and construction of a dipole antenna which met the conditions of the study previously conducted through simulations. Adapting the dimensions of the dipole antenna to correctly operate on frequency 434 MHz resulted in a successfully designed dipole with required loss power characteristics of -11 dB. In this thesis, the design of the dipole antenna element is primarily to demonstrate that the arrangement of antenna elements presented above (distances of individual antennas from each other) is based on real possibilities of how to spatially arrange antenna elements. In the case of an arrangement of 24 antennas, the distance between the individual antennas is 46 mm. The dimensions of the dipole presented by us are less than 30 mm, including the dielectric substrate. Avoidance of the balun has a clear advantage for clinical trials as

it has an impact on the quality of the reconstructed images in microwave imaging and thermometry [30; 37; 38].

When evaluating the obtained predictions of radiation characteristics of the dipole, we faced the common problem of the inability to define the quality of the SAR distribution in the tissue. The only evaluating parameter is a colourmap scale of SAR values from minimum to maximum deposited energy in W/kg. cSAR 3D measures the distribution of SAR in the plane 3 mm below the surface. For this reason, 3 curved peaks are not visible in the measurements as they appear in the simulations. (*Figure 5.20*). It is therefore necessary to compare these graphs just from the mentioned depth of 3 mm.

The results of this study may be further followed up by simulations in 3D models of the head with detailed structures. The other parameters of this model which would approximate real patients are perfusion caused by the circulation system of blood and convection of cerebrospinal fluid. These two factors would lower the EM energy deposited in the tissue and therefore would decrease the hyperthermic temperature. The aim would be to find the optimal settings of amplitude and phase for power steering of the antennas.

7 Conclusion

Using COMSOL Multiphysics and MATLAB software a 2D analysis of the antenna number and their operating frequency was held. The considered factor for the analyses was the ability to cover the whole target area, described as the Tumour Coverage factor, which is characterised as the percentage of the highest values of Specific Absorption Rate deposited in the human tissue. Another evaluated factor was the Hotspot-to Target Quotients which determines the ratio of the unwanted SAR coupling in the healthy tissue that causes unwanted heating in a target area. As expected, the lowest operating frequency studied met all the conditions that were required. As for the number of elements, it is concluded that at the frequency of 434 MHz, the 12-antenna hyperthermia system is capable of delivering sufficient power to the target area. Tested particle swarm optimisation appropriately localised the target areas by optimising the amplitude and phase of every antenna element of the HT system.

The ideal frequency obtained from the analyses was further used for the design of a dipole antenna in COMSOL. The parameters were adapted to fulfil the attributes of radiating elements used in a clinical environment. A reflection coefficient S_{11} met the requirement of delivering the power loss of -10 dB to the head tissue phantom.

The designed system can be used for tumours located in the 3cm rim of the brain tissue regardless of the lobe of incidence. Studied target sizes were from 20 mm to 30 mm, for this size range, our tested system satisfied the coverage of whole area. Performed analysis may be further tested for the detailed 3D models of the human head.

List of Literature

[1] DATTA, Niloy R., Susanne ROGERS, *Silvia Gómez ORDÓñEZ, Emsad* PURIC a Stephan BODIS**.** Hyperthermia and radiotherapy in the management of head and neck cancers: A systematic review and meta-analysis. *International Journal of Hyperthermia* [online]. 2016, **32**(1), 31-40 [cit. 2022-05-11]. ISSN 0265-6736. Dostupné z: doi:10.3109/02656736.2015.1099746

[2] ISSELS, Rolf D., Lars H. LINDNER, Jaap VERWEIJ et al. Effect of Neoadjuvant Chemotherapy Plus Regional Hyperthermia on Long-term Outcomes Among Patients With Localized *High-Risk Soft Tissue Sarcoma. JAMA Oncology [online]. 2018,* 4(4) [cit. 2022-05-11]. ISSN 2374-2437. Dostupné z: doi:10.1001/jamaoncol.2017.4996

[3] DATTA, N.R., S. ORDÓñEZ, U.S. GAIPL et al. Local hyperthermia combined with radiotherapy and-/or chemotherapy: Recent advances and promises *for the future*. Cancer Treatment Reviews [online**]**. 2015, 41(9), 742-753 [cit. 2022-05-05]. ISSN 03057372. Dostupné z: doi:10.1016/j.ctrv.2015.05.009

[4] DOBŠÍČEK TREFNÁ, Hana, Johannes CREZEE, Manfred SCHMIDT et al. Quality assurance guidelines for superficial hyperthermia clinical trials. Strahlentherapie und Onkologie *[*online]. 2017, 193(**5**), 351-366 [cit. 2022-05-11]. ISSN 0179-7158. Dostupné z: doi:10.1007/s00066-017-1106-0

[5] SAWICKI, James F., Jacob D. SHEA, Nader BEHDAD a Susan C. HAGNESS. The impact of frequency on the *performance of* microwave ablation. International Journal of Hyperthermia [online]. 2017, 33(1), 61-68 [cit. 2022-05-11]. ISSN 0265-6736. Dostupné z: doi:10.1080/02656736.2016.1207254

[6] LI, Jianian, Lifan XU a Xiong WANG. A Computational Study on Number of Elements in Antenna Array for Focused Microwave Breast Hyperthermia. In: 2019 IEEE MTT-S International Microwave Biomedical Conference (*IMBioC) [online]*. IEEE, 2019, s. 1-3 [cit. 2022-05-11]. ISBN 978-1-5386-7395-9. Dostupné z: doi:10.1109/IMBIOC.2019.8777809

[7] BLACK, Peter McL. Brain Tumors. New England Journal of Medicine [online]. 1991, 324(22), 1555-1564 [cit. 2022-05-11]. ISSN 0028-4793. Dostupné z: doi:10.1056/NEJM199105303242205

[8] LOUGHAN, Ashlee R., Deborah H. ALLEN, Karine BAUMSTARCK, Laurent BOYER, Pascal AUQUIER, Autumn LANOYE a Sarah BRAUN. Quality of Life *in* Neuro-Oncology. Handbook of Brain Tumor Chemotherapy, Molecular Therapeutics, and Immunotherapy [online]. Elsevier, 2018, s. 767-781 [cit. 2022-05-11]. ISBN 9780128121009. Dostupné z: doi:10.1016/B978-0-12-812100-9.00061-9

[9] MERCHANT, Thomas E., Ian F. POLLACK a Jay S. LOEFFLER. Brain Tumors Across the Age Spectrum: Biology, Therapy, and Late Effects. Seminars in Radiation Oncology *[online]*. 2010, 20(1), 58-66 [cit. 2022-05-11]. ISSN 10534296. Dostupné z: doi:10.1016/j.semradonc.2009.09.005

[10] D'ALESSIO, Alessio, Gabriella PROIETTI, Gigliola SICA a Bianca Maria SCICCHITANO. Pathological and Molecular Features of Glioblastoma and Its Peritumoral Tissue. Cancers [online]. 2019, 11*(4) [cit.* 2022-05-11]. ISSN 2072-6694. Dostupné z: doi:10.3390/cancers11040469

[11] LYNDON, Daniel, Joseph A. LANSLEY, Jane EVANSON a Anant *S. KRISHNAN. Dural masses: meningiomas and their mimics.* Insights into Imaging [online]. 2019, 10(1) [cit. 2022-05-11]. ISSN **1869-4101.** Dostupné z: doi:10.1186/s13244-019-0697-7

[12] LARJAVAARA, Suvi, Riitta MÄNTYLÄ, Tiina SALMINEN, Hannu HAAPASALO, Jani RAITANEN, Juha JÄÄSKELÄINEN a Anssi AUVINEN. Incidence of gliomas by anatomic location. Neuro-Oncology [online]. 2007, 9(3*)*, 319-325 [cit. *2022-05-12]*. ISSN 1523-5866. Dostupné **z**: doi:10.1215/15228517-2007-016

[13] PRABHAKAR, R, KP HARESH, T GANESH, RC JOSHI, PK JULKA a GK RATH. Comparison of computed *tomography and magnetic* resonance based target volume **in** brain tumors. Journal of Cancer Research and Therapeutics [online]. 2007, 3(2) [cit. 2022-05-12]. ISSN 0973-1482. Dostupné z: doi:10.4103/0973-1482.34694

[14] SKANDALAKIS, Georgios P., Daniel R. RIVERA, Caroline D. RIZEA, Alexandros BOURAS, Joe Gerald JESU RAJ, *Dominique BOZEC a* Constantinos G. HADJIPANAYIS. Hyperthermia treatment advances for brain tumors. International Journal of Hyperthermia [online]. 2020, 37(2), 3-19 [cit. 2022-05-11]. ISSN 0265-6736. Dostupné z: doi:10.1080/02656736.2020.1772512

[15] SNEED, Penny K., Paul R. STAUFFER, Michael W. MCDERMOTT et al. Survival benefit of hyperthermia *in a prospective randomized* trial of brachytherapy boost ± hyperthermia for glioblastoma multiforme. International

Journal of Radiation Oncology*Biology*Physics [online]. 1998, 40(2), 287-295 [cit. 2022-05-05]. ISSN 03603016. Dostupné z: doi:10.1016/S0360-3016(97)00731-1

[16] HANNON, Gary, Felista L. TANSI, Ingrid HILGER a Adriele PRINA-MELLO. The Effects of Localized Heat *on the Hallmarks of* Cancer. Advanced Therapeutics **[**online]. 2021, 4(7) [cit. 2022-05-05]. ISSN 2366-3987. Dostupné z: doi:10.1002/adtp.202000267

[17] D'ANDREA, John A., John M. ZIRIAX a Eleanor R. ADAIR. Radio frequency electromagnetic fields: mild *hyperthermia and safety standards*. Neurobiology of Hyperthermia **[**online]. Elsevier, 2007, s. 107-135 [cit. 2022-05-11]. Progress in Brain Research. ISBN 9780444519269. Dostupné z: doi:10.1016/S0079-6123(06)62007-4

[18] PAULIDES, M.M., H. DOBSICEK TREFNA, S. CURTO a D.B. RODRIGUES. Recent technological advancements *in radiofrequency-andmicrowave-mediated* hyperthermia for enhancing drug **delivery**. Advanced Drug Delivery Reviews [online]. 2020, 163-164, 3-18 [cit. 2022-05-04]. ISSN 0169409X. Dostupné z: doi:10.1016/j.addr.2020.03.004

[19] HASGALL, PA, F DI GENNARO, C BAUMGARTNER et al. IT'IS Database for thermal and electromagnetic parameters of *biological tissues,*. Version 4.1. 2022. DOI: 10.13099/VIP21000-04-1. Dostupné také z: itis.swiss/database

[20] KOK, H., C. VAN DEN BERG, A. BEL a J. CREZEE. Fast thermal simulations and *temperature optimization for* hyperthermia treatment planning, including realistic 3D vessel networks. Medical Physics [online]. 2013, 40(10) [cit. 2022-05-04]. ISSN 00942405. Dostupné z: doi:10.1118/1.4821544

[21] VAN RHOON, Gerard C. Is CEM43 still a relevant thermal dose parameter for hyperthermia treatment monitoring?. International *Journal of Hyperthermia* [online]. 2016, 32**(**1), 50-62 [cit. 2022-05-12]. ISSN 0265-6736. Dostupné z: doi:10.3109/02656736.2015.1114153

[22] BELLIZZI, Gennaro G., Tomas DRIZDAL, Gerard C. VAN RHOON, Lorenzo CROCCO, Tommaso ISERNIA a Margarethus *M. PAULIDES. Predictive* value of SAR based quality indicators for head and neck hyperthermia treatment quality. International Journal of Hyperthermia [online]. 2019, 36(1), 455-464 [cit. 2022-05-12]. ISSN 0265-6736. Dostupné z: doi:10.1080/02656736.2019.1590652

[23] KEITH D. PAULSEN, SHIREEN GEIMER, J. Optimization of pelvic heating rate distributions with electromagnetic phased arrays. *International Journal of Hyperthermia* [online]. 2009, **15**(3), 157-186 [cit. 2022-05-08]. ISSN 0265-6736. Dostupné z: doi:10.1080/026567399285701

[24] 2D simulation of the electromagnetic wave across the non-uniform reentry plasma sheath with COMSOL. AIP Advances [online]. *2019, 9(5)* [cit. 2022-05-12]. ISSN 2158-3226. Dostupné z: doi:10.1063/1.5085876

[25] GAS, Piotr. SAR optimization for multi-dipole antenna array with regard to local hyperthermia. PRZEGLĄD ELEKTROTECHNICZNY [online]. 2019, 1(1), 19-22 [cit. 2022-05-12]. ISSN 0033-2097. Dostupné z*: doi:10.15199/48.2019.01.05*

[26] RODRIGUES, Dario B., Jason ELLSWORTH a Paul TURNER. Feasibility of Heating Brain Tumors Using a 915 MHz *Annular Phased-Array. IEEE* Antennas and Wireless Propagation Letters [online]. 2021, 20(4), 423-427 [cit. 2022-05-11]. ISSN 1536-1225. Dostupné z: doi:10.1109/LAWP.2021.3050142

[27] JORET, Ariffuddin, Nur Izzati ZULKEFLI, Samsul Haimi DAHLAN, Siti Hajar AMINAH ALI, Muhammad Suhaimi SULONG a *Maryanti RAZALI. Dipole* antenna design as hyperthermia **applicator** using CST microwave studio. International Journal of Biosensors & Bioelectronics [online]. 2021, 7(2) [cit. 2022-05-12]. ISSN 25732838. Dostupné z: doi:10.15406/ijbsbe.2021.07.00209

[28] YEOH, W.S., K.L. WONG a W.S.T. ROWE. Miniaturized half-bowtie printed dipole antenna *with an integrated* balun. In: 2008 **Asia-Pacific** Microwave Conference [online]. IEEE, 2008, s. 1-4 [cit. 2022-05-11]. ISBN 978-1-4244-2641-6. Dostupné z: doi:10.1109/APMC.2008.4958546

[29] KAZEMIPOUR, ALIREZA a XAVIER BEGAUD. Calculable Dipole Antenna for EMC Measurements with Low-Loss Wide-Band Balun from 30 MHz to 2 GHz. *Electromagnetics* [online]. 2005, **25**(3), 187-202 [cit. 2022-05-11]. ISSN 0272-6343. Dostupné z: doi:10.1080/02726340590915584

[30] WUST, Peter, Horst FÄHLING, Waldemar WLODARCZYK, Martin SEEBASS, Johanna GELLERMANN, Peter DEUFLHARD a Jacek NADOBNY. *Antenna arrays in the* SIGMA-eye applicator: Interactions **and** transforming networks. Medical Physics [online]. 2001, 28(8), 1793-1805 [cit. 2022-05-11]. ISSN 00942405. Dostupné z: doi:10.1118/1.1388220

[31] CSAR3D V3.1 Manual. Schmid & Partner Engineering AG. . Https://speag.swiss/.

[32] LEE, Sun-Young, Giammaria FIORENTINI, Attila Marcell SZASZ, Gyula SZIGETI, Andras SZASZ a Carrie Anne MINNAAR. Quo *Vadis Oncological Hyperthermia* (2020)?. Frontiers **in** Oncology [online]. 2020, 10 [cit. 2022-05-12]. ISSN 2234-943X. Dostupné z: doi:10.3389/fonc.2020.01690

[33] VERDUIJN, G. M., E. M. DE WEE, Z. RIJNEN et al. Deep hyperthermia with *the HYPERcollar system combined* with irradiation for advanced head and neck carcinoma – a feasibility study. International Journal of Hyperthermia [online]. 2018, 34(7), 994-1001 [cit. 2022-05-12]. ISSN 0265-6736. Dostupné z: doi:10.1080/02656736.2018.1454610

[34] BAKKER, Akke, Remko ZWEIJE, Henny Petra KOK, Merel Willemijn KOLFF, H. J. G. Desiree VAN *DEN BONGARD, Manfred* SCHMIDT, Geertjan VAN **TIENHOVEN** a Hans CREZEE. Clinical Feasibility of a High-Resolution Thermal Monitoring Sheet for Superficial Hyperthermia in Breast Cancer Patients. Cancers [online]. 2020, 12(12) [cit. 2022-05-12]. ISSN 2072-6694. Dostupné z: doi:10.3390/cancers12123644

[35] JOUVIE, F., J.-C. BOLOMEY a G. GABORIAUD. Discussion of Capabilities of Microwave Phased Arrays for *Hyperthermia Treatment of* Neck Tumors. IEEE Transactions on Microwave Theory and Techniques [online]. 1986, 34(5), 495-501 [cit. 2022-05-12]. ISSN 0018-9480. Dostupné z: doi:10.1109/TMTT.1986.1133382

[36] PAULIDES, Margarethus M., Stefan H.J.A. VOSSEN, Adrianus P.M. ZWAMBORN a Gerard C. *VAN RHOON. Theoretical* investigation into the feasibility **to** deposit RF energy centrally in the head-and-neck region. International Journal of Radiation Oncology*Biology*Physics [online]. 2005, 63(2), 634-642 [cit. 2022-05-12]. ISSN 03603016. Dostupné z: doi:10.1016/j.ijrobp.2005.04.048

[37] GHADERI ARAM, Morteza, Larisa BEILINA a Hana DOBSICEK TREFNA. Microwave thermometry with potential application in non-invasive monitoring *of hyperthermia*. *Journal* of Inverse and Ill-posed **Problems** [online]. 2020, 28(5), 739-750 [cit. 2022-05-11]. ISSN 1569-3945. Dostupné z: doi:10.1515/jiip-2020-0102

[38] GHADERI ARAM, Morteza, Hadi ALIAKBARIAN a Hana DOBŠÍČEK TREFNÁ. An ultra-wideband compact design for hyperthermia: Open *ridged-waveguide antenna*. IET Microwaves, Antennas **&** Propagation [online]. 2022, 16(2-3), 137-152 [cit. 2022-05-11]. ISSN 1751-8725. Dostupné z: doi:10.1049/mia2.12226

Appendix A

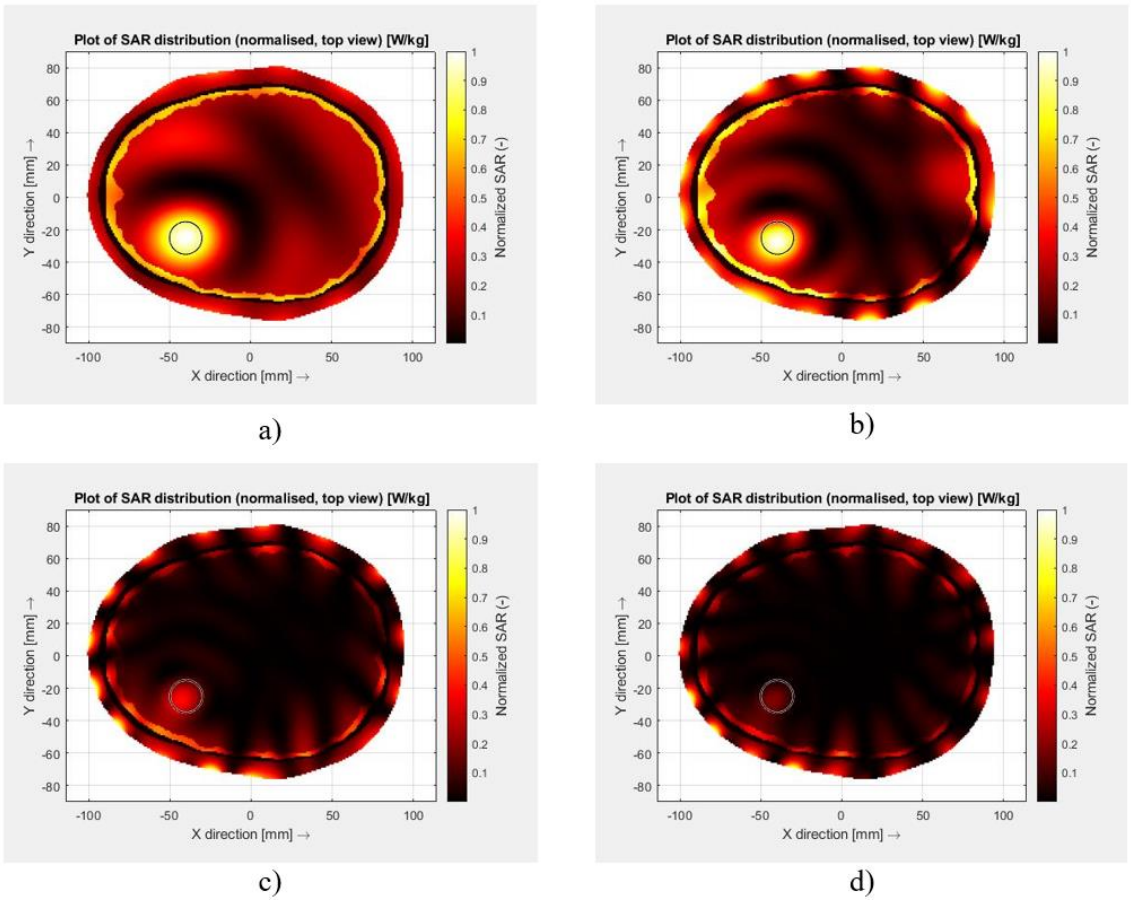

Figure A 1: SAR distribution in the 2D head model obtained by a 16-antenna HT system on the frequency of a) 434 MHz, b) 650 MHz, c) 915 MHz and d) 1150 MHz

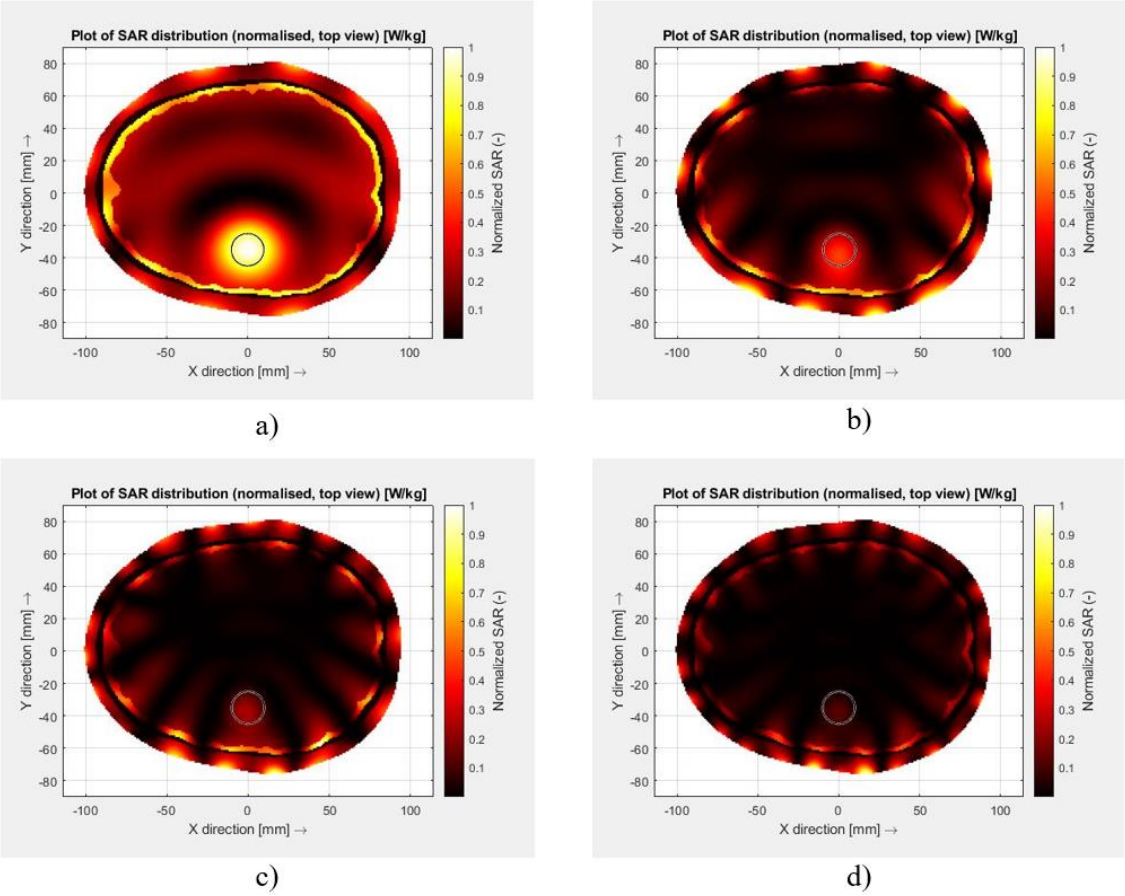

Figure A 2: SAR distribution in the 2D head model obtained by a 12-antenna HT system on the frequency of a) 434 MHz, b) 650 MHz, c) 915 MHz and d) 1150 MHz

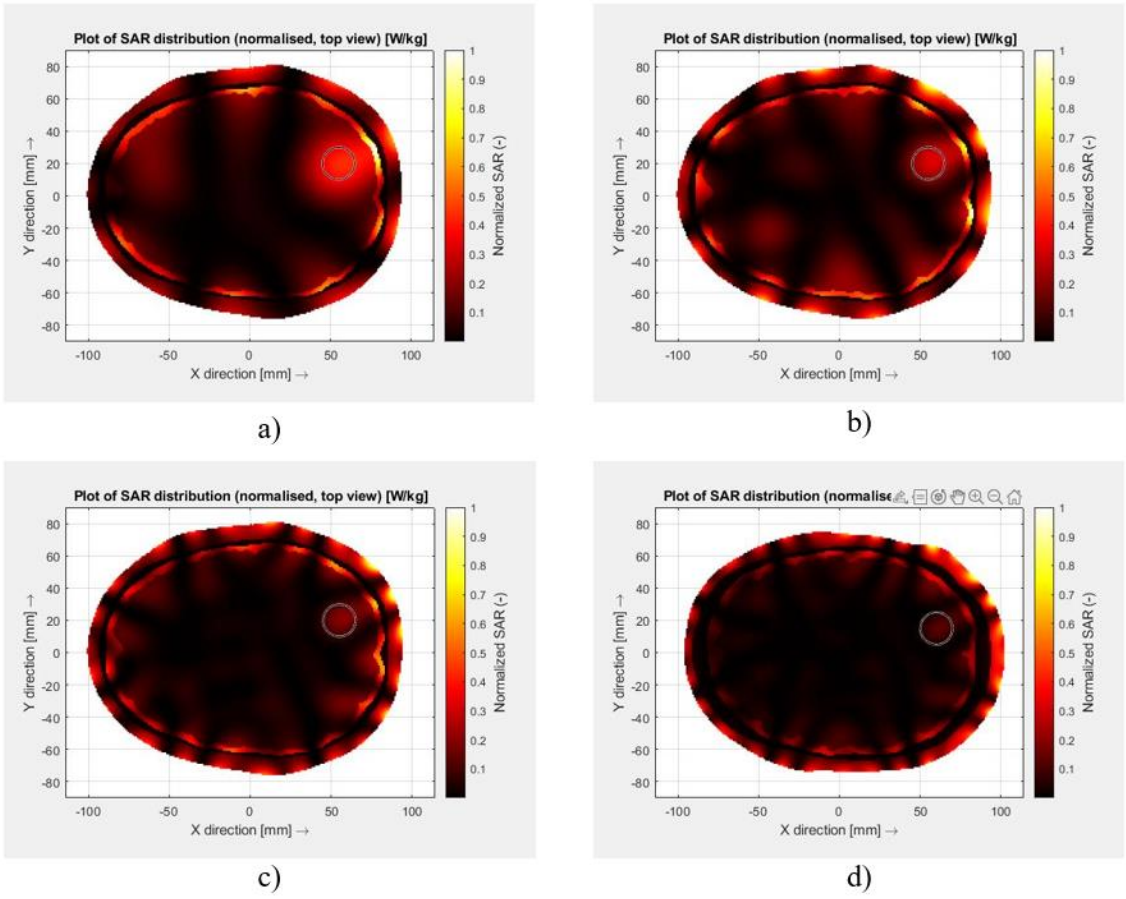

Figure A 3: SAR distribution in the 2D head model obtained by a 8-antenna HT system on the frequency of a) 434 MHz, b) 650 MHz, c) 915 MHz and d) 1150 MHz

Appendix B

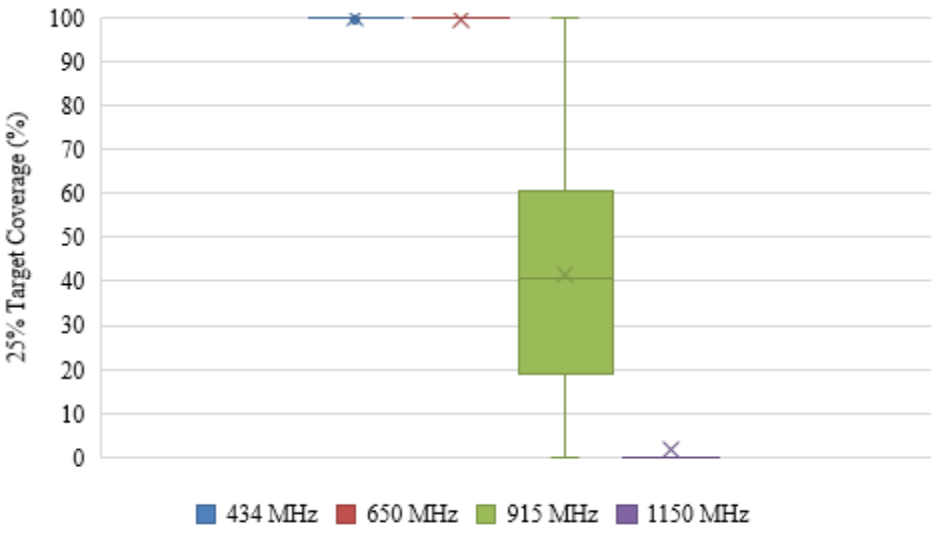

Figure B 1: Box plot of TC25 comparing four frequencies used for a 16-antenna HT system. Mean values are represented by a cross

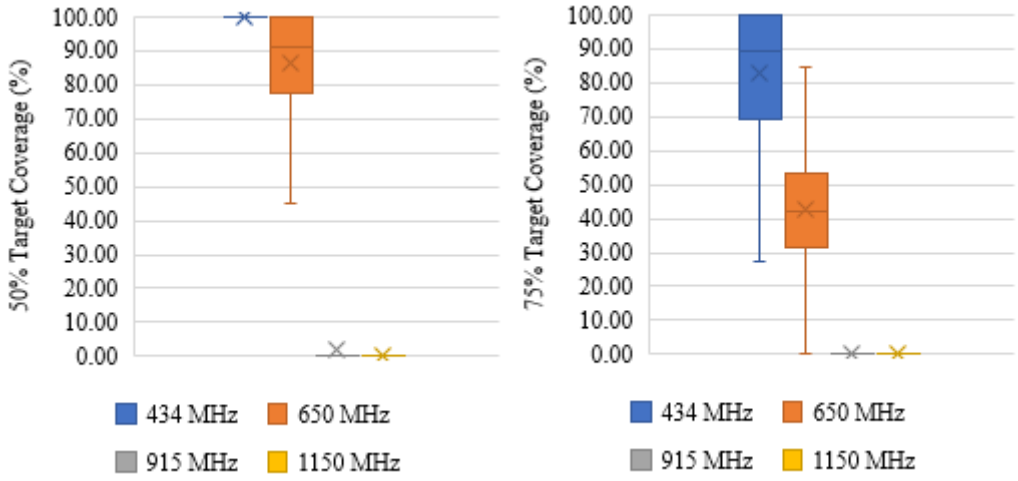

Figure B 2: Box plot of TC50 & TC75 comparing four frequencies used for a 16-antenna HT system. Mean values are represented by a cross

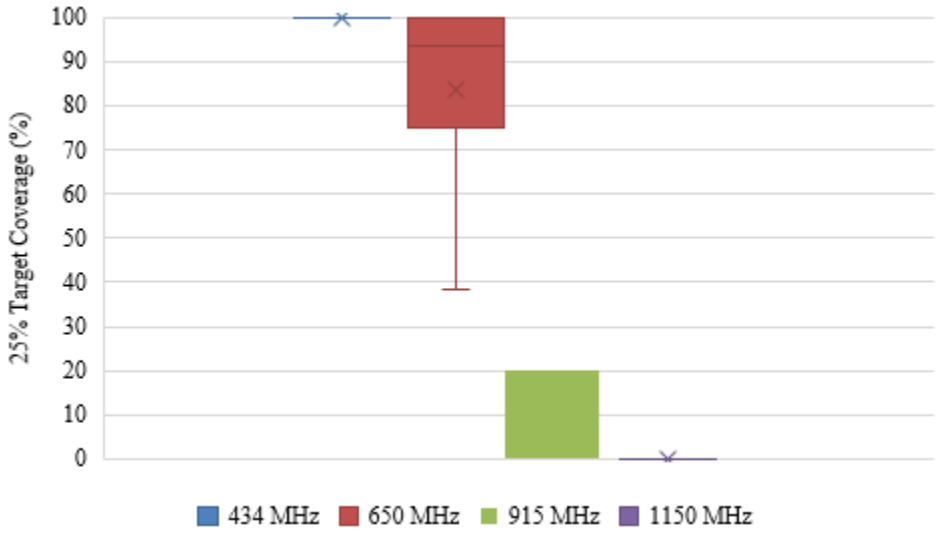

Figure B 3: Box plot of TC25 comparing four frequencies used for a 12-antenna HT system. Mean values are represented by a cross

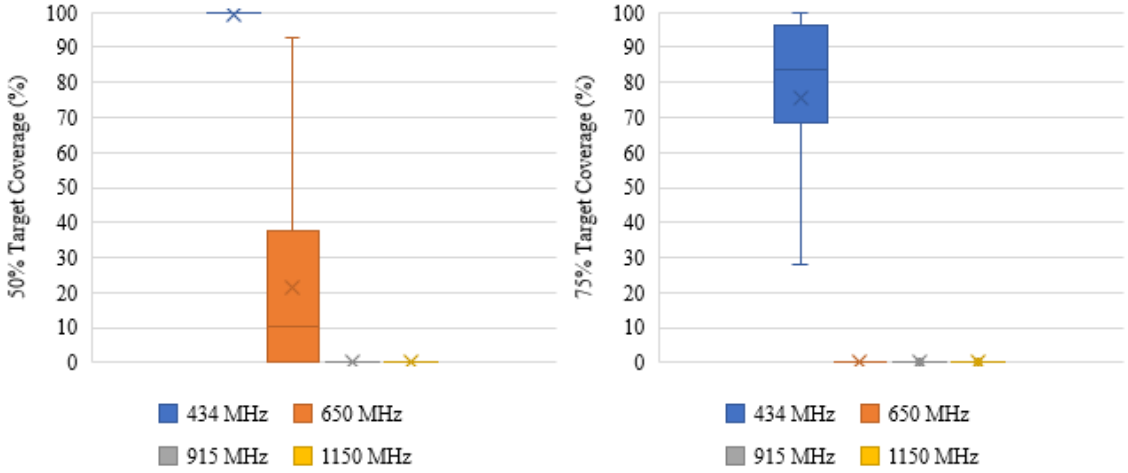

Figure B 4: Box plot of TC50 & TC75 comparing four frequencies used for a 12-antenna HT system. Mean values are represented by a cross

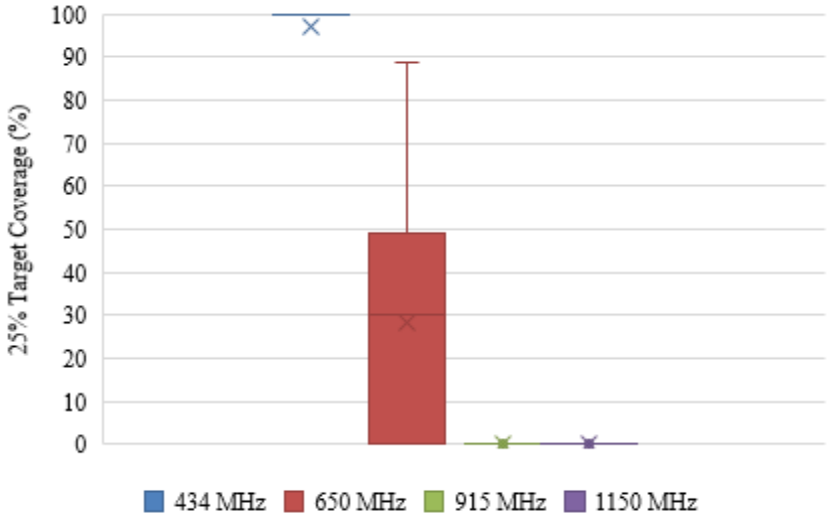

Figure B 5: Box plot of TC25 comparing four frequencies used for a 8-antenna HT system. Mean values are represented by a cross

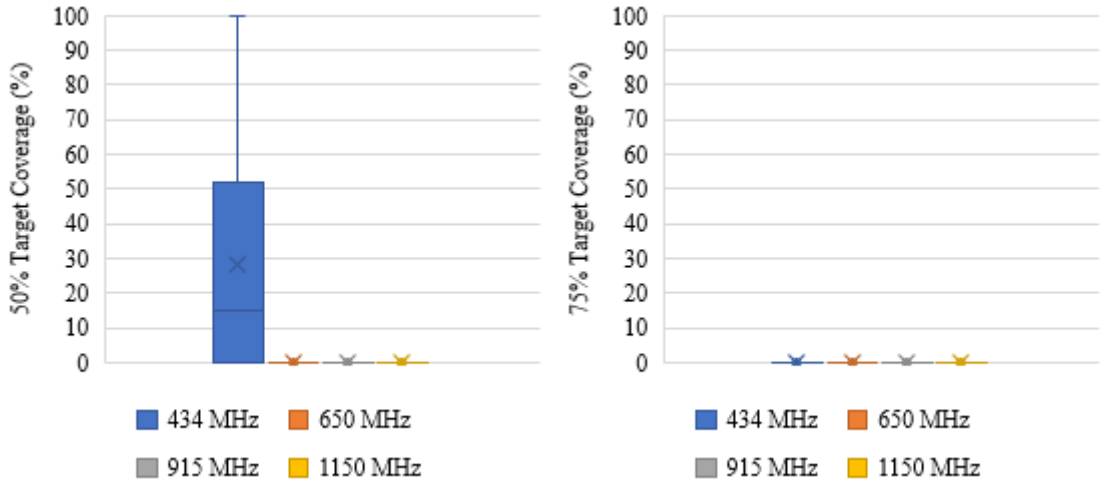

Figure B 6: Box plot of TC50 & TC75 comparing four frequencies used for a 8-antenna HT system. Mean values are represented by a cross

Appendix C:

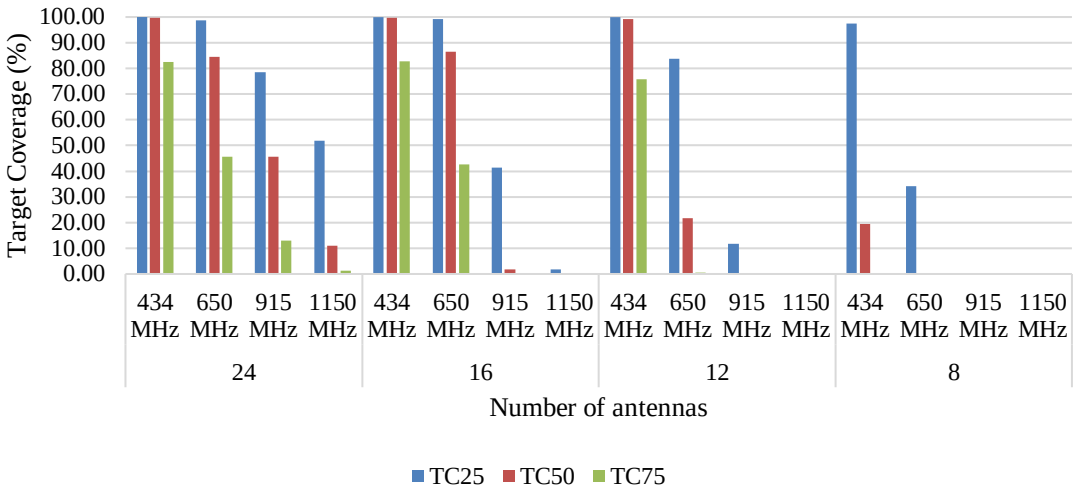

Figure C 1: Target Coverage comparison for four antenna number of the HT system operating at the frequencies 434 MHz, 650 MHz, 915 MHz and 1150 MHz

Appendix D: Content of the annex

- MATLAB codes for optimisation of HTQ parameters, phase, and amplitude
- COMSOL file with antenna design
- Figures of 4800 simulation results
- Excel file with the measured values of HTQ, TC25, TC50, TC75, Amplitude, & Phase for every simulation